Molecular Therapy
Original Article

ESC-sEVs Rejuvenate Aging Hippocampal NSCs by Transferring SMADs to Regulate the MYT1-Egln3-Sirt1 Axis

Guowen Hu,[1,2,4] Yuguo Xia,[1,4] Bi Chen,[3] Juntao Zhang,[3] Liangzhi Gong,[3] Yu Chen,[3] Qing Li,[3] Yang Wang,[3] and Zhifeng Deng[1]

[1]Department of Neurosurgery, Shanghai Jiao Tong University Affiliated Sixth People's Hospital, Shanghai 200233, China; [2]Department of Neurosurgery, The Second Affiliated Hospital of Nanchang University, Nanchang 330006, China; [3]Institute of Microsurgery on Extremities, Shanghai Jiao Tong University Affiliated Sixth People's Hospital, Shanghai 200233, China

Tissue stem cell senescence leads to stem cell exhaustion, which results in tissue homeostasis imbalance and a decline in regeneration capacity. However, whether neural stem cell (NSC) senescence occurs and causes neurogenesis reduction during aging is unknown. In this study, mice at different ages were used to detect age-related hippocampal NSC (H-NSC) senescence, as well as the function and mechanism of embryonic stem cell-derived small extracellular vesicles (ESC-sEVs) in rejuvenating H-NSC senescence. We found a progressive cognitive impairment, as well as age-related H-NSC senescence, in mice. ESC-sEV treatment significantly alleviated H-NSC senescence, recovered compromised self-renewal and neurogenesis capacities, and reversed cognitive impairment. Transcriptome analysis revealed that myelin transcription factor 1 (MYT1) is downregulated in senescent H-NSCs but upregulated by ESC-sEV treatment. In addition, knockdown of MYT1 in young H-NSCs accelerated age-related phenotypes and impaired proliferation and differentiation capacities. Mechanistically, ESC-sEVs rejuvenated senescent H-NSCs partly by transferring SMAD family members 4 (SMAD4) and 5 (SMAD5) to activate MYT1, which downregulated egl-9 family hypoxia inducible factor 3 (Egln3), followed by activation of hypoxia inducible factor 2 subunit α (HIF-2α), nicotinamide phosphoribosyl transferase (NAMPT), and sirtuin 1 (Sirt1) successively. Taken together, our results indicated that H-NSC senescence caused cellular exhaustion, neurogenesis reduction, and cognitive impairment during aging, which can be reversed by ESC-sEVs. Thus, ESC-sEVs may be promising therapeutic candidates for age-related diseases.

INTRODUCTION

With the increase of lifespan, aging populations are progressively growing, which is also accompanied by an increased risk of age-related neurodegenerative diseases, including Alzheimer's disease (AD) and Parkinson's disease (PD), causing severe social and economic burdens.[1] Adult neurogenesis mainly occurs in the subventricular zone (SVZ) of the lateral ventricle and dentate gyrus (DG) of the hippocampus and declines gradually with age,[2,3] primarily due to the loss of the proliferative capability of neural stem cells (NSCs),[4] consequently giving rise to age-related memory loss and cognitive dysfunction. Cellular senescence, which is defined as an essentially irreversible cell cycle arrest caused by various biological and pathological conditions, has been demonstrated to account for tissue homeostasis impairment.[5] Age-associated stem cell senescence has been confirmed as an important part of the pathogenesis of multiple disorders.[6] For example, hematopoietic stem cells became senescent gradually with aging, lost their self-renewal and regenerative potential, and weakened the adaptive immune system.[7] Multiple studies have demonstrated that NSC senescence was associated with the loss of stem cell markers,[8] as well as self-renewal and neurogenic capacity impairment.[9–11] However, whether NSCs undergo the senescence process with natural aging, the potential underlying mechanism, and the relationship with neurogenesis are not well elucidated.

Rejuvenation of stem cell senescence can enhance their self-renewal and regenerative capacities, which has been proposed as a promising therapeutic approach to restore tissue structure and function.[6] For example, rejuvenation of senescent oligodendrocyte progenitor cells by fasting or metformin can restore the differentiation potential as well as remyelination ability.[12] Small extracellular vesicles (sEVs) are natural nanosized particles that participate in intracellular

Received 17 March 2020; accepted 28 September 2020;
https://doi.org/10.1016/j.ymthe.2020.09.037.

[4]These authors contributed equally to this work.

Correspondence: Zhifeng Deng, Department of Neurosurgery, Shanghai Jiao Tong University Affiliated Sixth People's Hospital, 600 Yishan Road, Shanghai 200233, China.
E-mail: zfdeng@sjtu.edu.cn
Correspondence: Yang Wang, Institute of Microsurgery on Extremities, Shanghai Jiao Tong University Affiliated Sixth People's Hospital, 600 Yishan Road, Shanghai 200233, China.
E-mail: wangyang63@sjtu.edu.cn
Correspondence: Qing Li, Institute of Microsurgery on Extremities, Shanghai Jiao Tong University Affiliated Sixth People's Hospital, 600 Yishan Road, Shanghai 200233, China.
E-mail: liqing_236@aliyun.com

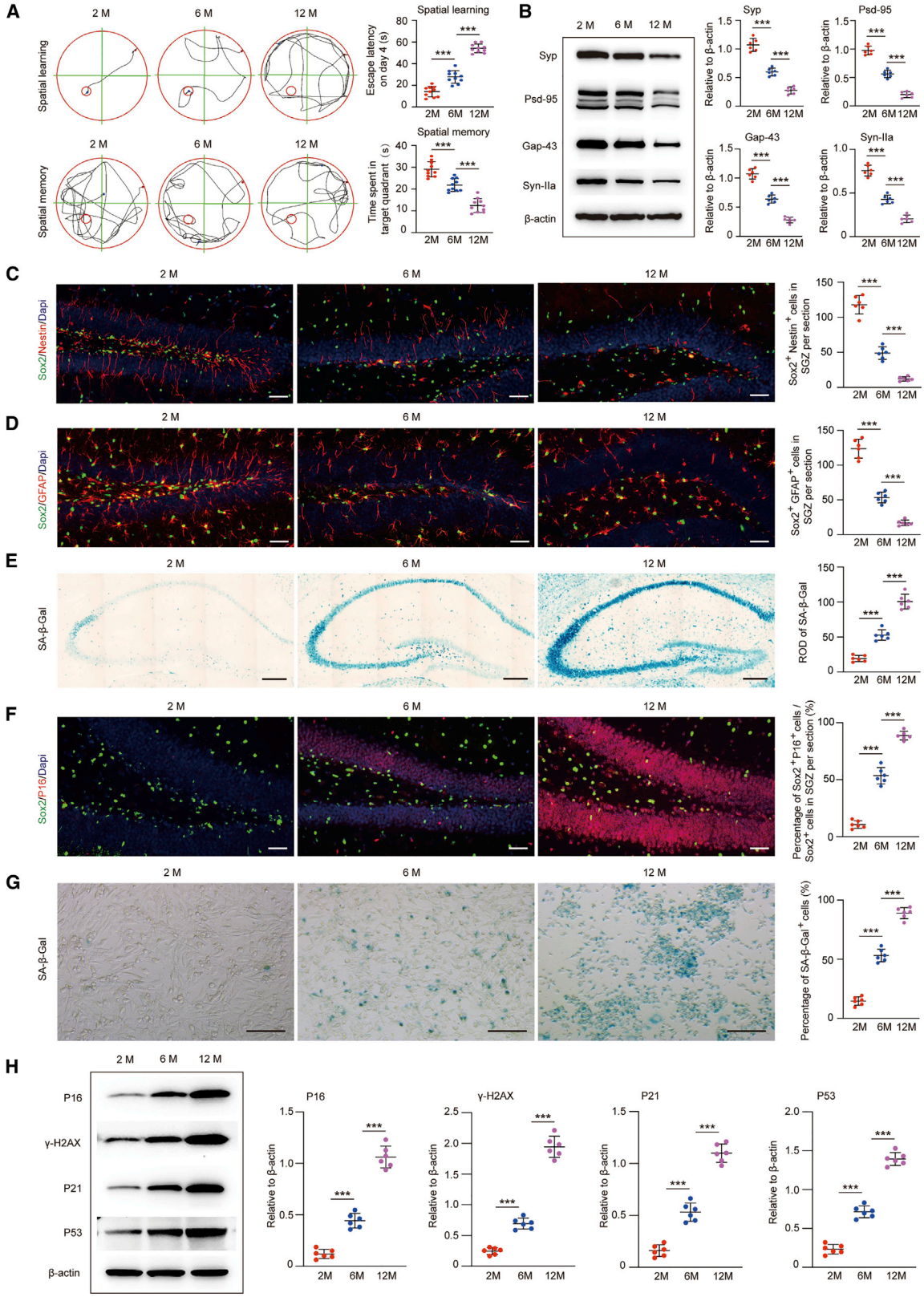

(legend on next page)

communication and influence the behavior of recipient cells via the delivery of functional biomolecules.[13] Stem cell-derived sEVs are regarded as an attractive therapeutic strategy in regenerative medicine due to their promising pro-regenerative effects, no risk of aneuploidy, and low possibility of immune rejection.[14–16] Embryonic stem cell-derived sEVs (ESC-sEVs) contain bioactive factors from their parental cells that possess unique capacities, including infinite proliferation ability, pluripotency, and an intrinsic youthful barrier to aging,[17] suggesting they may be beneficial for treating aging-associated disease. Recent studies from our group and others have demonstrated that ESC-sEVs can rejuvenate somatic cell senescence and promote regeneration,[18,19] suggesting they may be beneficial to aging-associated disease.

In this study, we reported that hippocampal NSC (H-NSC) senescence is accompanied by the progression of aging. Myelin transcription factor 1 (MYT1) is downregulated in senescent H-NSCs, and knockdown of MYT1 in young H-NSCs promotes age-related phenotypes and impairs proliferation as well as differentiation capacities. We also found that ESC-sEVs can rejuvenate senescent H-NSCs partly by transferring SMAD family members 4 (SMAD4) and 5 (SMAD5) to activate MYT1, inhibiting egl-9 family hypoxia inducible factor 3 (Egln3) expression, improving hypoxia inducible factor 2 subunit α (HIF-2α) levels, promoting nicotinamide phosphoribosyl transferase (NAMPT) expression, and upregulating sirtuin 1 (Sirt1). In this study, for the first time, we identify a MYT1-dependent transcriptional program involved in H-NSC senescence that contributed to cognitive impairment with aging. We also demonstrate that ESC-sEVs have the potential to reverse cognitive dysfunction by rejuvenating H-NSC senescence.

RESULTS

Hippocampal NSCs Exhibited a Senescent Phenotype with Aging

In this study, senescence-accelerated mouse prone 8 (SAMP8) mice were used to evaluate H-NSC senescence with aging. As cognitive aging is a lifelong process of ongoing and progressive cognitive functional decline in the senior,[20] we first evaluated the spatial learning and memory abilities of SAMP8 mice of different ages (2 months, young; 6 months, middle-aged; 12 months, aged) using a Morris water maze (MWM). As shown in Figure 1A, the escape latency on day 4 was markedly increased from the 2 month group to the 12 month group. The time spent in the target quadrant on day 5 was gradually decreased from the 2 month group to the 12 month group. As synaptic plasticity is the neurobiological basis of cognitive function,[21] we then detected the expression of hippocampal synapse-related proteins, including synaptophysin (Syp), postsynaptic density protein-95 (PSD-95), growth-associated protein-43 (Gap-43), and synapsin IIa (Syn-IIa). As shown in Figure 1B, among the three groups, the expression level of Syp, PSD-95, Gap-43, and Syn-IIa decreased significantly with the increase in age. These data confirmed an age-related reduction of cognitive function in mice.

As H-NSCs play a crucial role in maintaining and restoring cognition, their loss directly leads to the decline of neuroplasticity and cognitive function.[22,23] We calculated the number of H-NSCs in the subgranular zone (SGZ) among the three groups. Antibodies against Sox2 and Nestin as well as Sox2 and glial fibrillary acidic protein (GFAP) were used to label H-NSCs. As shown in Figures 1C and 1D, Sox2 and Nestin coexpressing cells as well as Sox2 and GFAP coexpressing cells were found to be densely present in the SGZ of 2 month mice, and the gradually diminished with an increase of age. The number of $Sox2^+$/$Nestin^+$ and $Sox2^+$/$GFAP^+$ NSCs in the 6 month group was significantly lower than that in the 2 month group, and these cells almost disappeared in 12 month mice. We further isolated H-NSCs from different ages of mice, and we found that the neurosphere size (Figure S1A) and β-tubulin III^+ cells (Figure S1B) decreased with the increase of age in mice, meaning that the proliferation and neuronal differentiation abilities of H-NSCs decreased with aging. In addition, the correlation analysis showed that the numbers of $Sox2^+$/$Nestin^+$ cells and $Sox2^+$/$GFAP^+$ cells in the SGZ were negatively correlated with escape latency on day 4, and positively correlated with the time spent in the target quadrant on day 5, with the expression level of hippocampal synapse-related proteins (Syp, PSD-95, Gap-43, Syn-IIa) (Figure S2). Overall, the age-dependent loss of H-NSCs correlated well with age-related cognitive function decline, which led us to investigate the internal change of H-NSCs with aging.

Since stem cells could become senescent with aging, which impairs their intrinsic functions,[6] we further detected the senescent status of H-NSCs in mice of different ages. As shown in Figure 1E, compared to the 2 month group, the activity of senescence-associated β-galactosidase (SA-β-gal) gradually increased in the hippocampus in the 6 month and 12 month group. These results indicated an aggravation of hippocampal senescence with aging in mice. Then, we performed

Figure 1. Cognitive Impairment, H-NSC Depletion, and Senescence in SAMP8 Mice during Aging

(A) Spatial learning and memory abilities in mice at an age of 2, 6, and 12 months were tested by the MWM. n = 10 per group. ***p < 0.001. (B) Western blot analysis and quantification of Syp, Gap-43, PSD-95, and Syn-IIa (relative to β-actin) in the hippocampus of mice at an age of 2, 6, and 12 months. n = 6 per group. ***p < 0.001. (C) IF images for $Sox2^+$ (green) and $Nestin^+$ (red) cells and the number of $Sox2^+$/$Nestin^+$ double-stained cells in the SGZ of mice at an age of 2, 6, and 12 months. Scale bars, 50 μm. n = 6 per group. ***p < 0.001. (D) IF images for $Sox2^+$ (green) and $GFAP^+$ (red) cells and the number of $Sox2^+$/$GFAP^+$ double-stained cells in the SGZ of mice at an age of 2, 6, and 12 months. Scale bars, 50 μm. n = 6 per group. ***p < 0.001. (E) SA-β-gal staining of the hippocampus and quantification of hippocampal SA-β-gal activity in mice at an age of 2, 6, and 12 months. Scale bars, 250 μm. n = 6 per group. ***p < 0.001. (F) IF images of $p16^{INK4a+}$ (red)/$Sox2^+$ (green) senescent H-NSCs and the quantification of $Sox2^+$/$p16^{INK4a+}$ double-stained cells of all $Sox2^+$ cells in the SGZ of mice at an age of 2, 6, and 12 months. Scale bars, 50 μm. n = 6 per group. ***p < 0.001. (G) Representative images of SA-β-gal staining and quantification of SA-β-gal^+ cells from isolated H-NSCs from SAMP8 mice at an age of 2, 6, and 12 months. Scale bars, 100 μm. n = 6 per group. ***p < 0.001. (H) Western blot analysis and quantification of $p16^{INK4a}$, γ-H2AX, p21, and p53 in isolated neurospheres in SAMP8 mice at an age of 2, 6, and 12 months. n = 6 per group. ***p < 0.001.

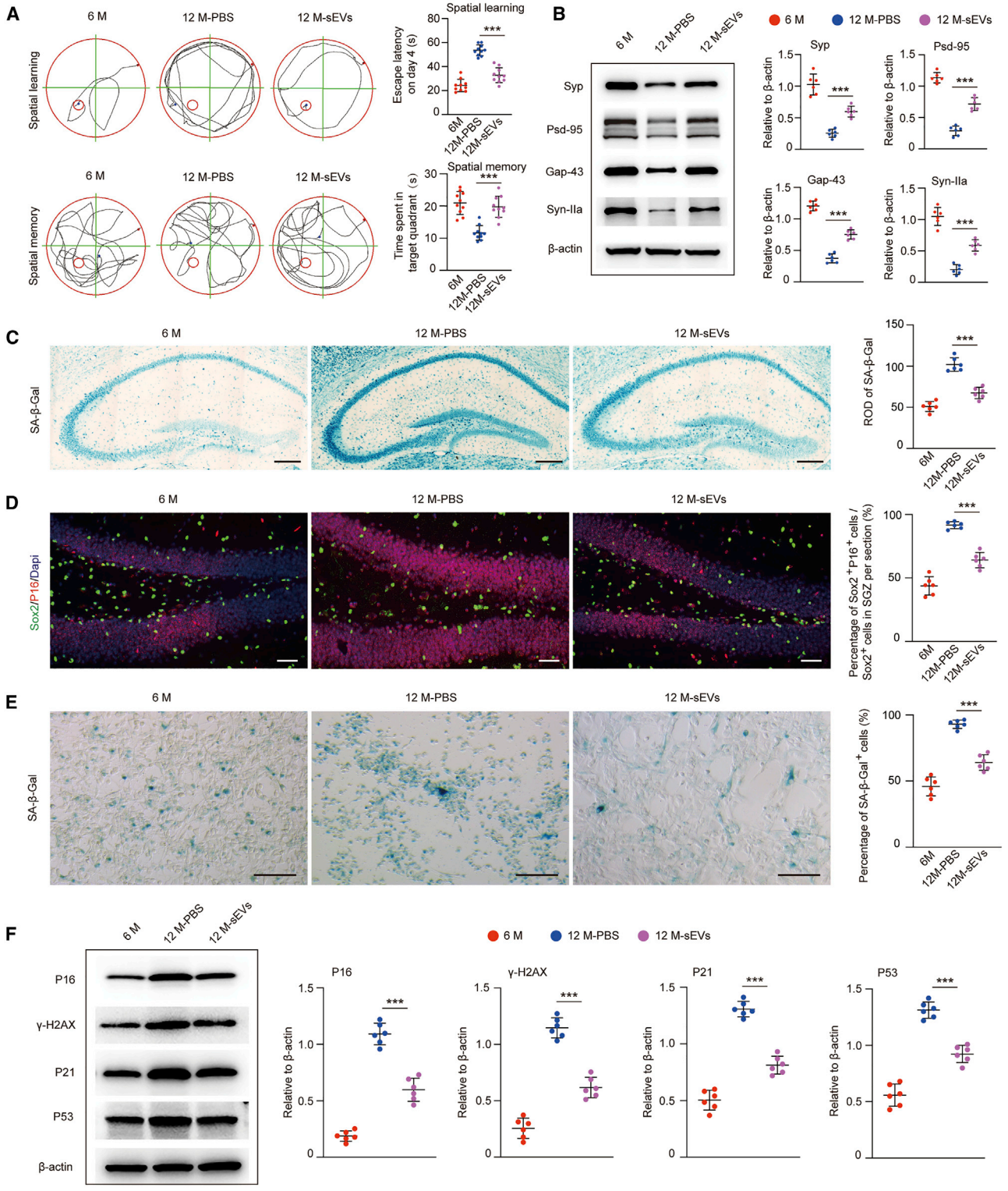

Figure 2. ESC-sEVs Reverse Cognitive Aging and Rejuvenate H-NSC Senescence in SAMP8 Mice

(A) Spatial learning and memory abilities were tested by an MWM test in 6 month, 12 month-PBS, and 12 month-sEV mice. n = 10 per group. ***p < 0.01. (B) Western blot analysis and quantification of Syp, Gap-43, PSD-95, and Syn-IIa in hippocampus of 6 month, 12 month-PBS, and 12 month-sEV mice. n = 6 per group. ***p < 0.001. (C) SA-

(legend continued on next page)

$p16^{INK4a}$ (senescence marker) and Sox2 (NSC marker) double staining to identify senescent NSCs in the hippocampus. As shown in Figure 1F, among the three groups, the percentage of Sox2 and $p16^{INK4a}$ coexpressing cells of the total $Sox2^+$ cells in the SGZ was the lowest in the 2 month group, and gradually increased with age. Additionally, we isolated H-NSCs from the hippocampus of mice at different ages, and we found that the percentage of SA-β-gal^+ cells gradually increased from 2 months to 12 months (Figure 1G). Moreover, the expression level of senescence-related proteins ($p16^{INK4a}$, γ-H2AX, p21, and p53) in isolated hippocampal neurospheres also gradually increased with age (Figure 1H). Taken together, these findings indicated an age-related H-NSC senescence in mice and suggested that H-NSC senescence during aging may result in loss of H-NSCs and subsequently cognitive dysfunction.

ESC-sEVs Ameliorate Hippocampal NSC Senescence and Enhanced NSC Activity in SAMP8 Mice during Aging

As described above, H-NSC senescence could be an important reason for the loss of H-NSCs during aging. Thus, amelioration of H-NSC senescence may reverse hippocampal neurogenesis reduction and cognitive impairment. In our previous study, we demonstrated that ESC-sEVs possessed an excellent ability to rejuvenate endothelial senescence.[19] Therefore, we explored whether ESC-sEVs could rejuvenate H-NSC senescence during aging. As shown in Figures S3A and S3B, ESC colonies were identified by the expression of alkaline phosphatase (ALP) and pluripotency-related markers, including OCT4, Nanog, TRA-1-81, TRA-1-60, and SSEA4. Then, ESC-sEVs were purified from the conditioned medium (CM). ESC-sEVs exhibited a size distribution of approximately 100 nm with a characteristic cup-shaped morphology under transmission electron microscopy (TEM) (Figure S3C). Flow nanoanalyzer analysis indicated particles with a mean diameter of 70.3 ± 17.7 nm and a concentration of $1.82 \times 10^{11} \pm 0.17 \times 10^{11}$ particles/mL (Figure S3D). Western blot showed that ESC-sEVs express exosomal markers CD9, CD63, and TSG101, but not the Golgi matrix protein GM130, β-actin, and Lamin A/C (Figure S3E), which means there was no contamination of cellular components in the isolated ESC-sEVs. We further evaluated the yield of ESC-sEVs by particle concentration and protein concentration. As shown in Figures S3F–S3I, the mean particle concentration was $7.06 \times 10^8 \pm 0.93 \times 10^8$ particles/mL in CM and 817.92 ± 94.13 particles/cell. The mean protein concentration was 1,127.49 ± 81.47 ng/mL in CM and $11.43 \times 10^{-7} \pm 1.57 \times 10^{-7}$ ng/particle. All relevant data of our experiments have been submitted to the EV-TRACK knowledgebase (EV-TRACK ID: EV200069).[24]

Next, ESC-sEVs were injected intravenously into 6-month-old male SAMP8 mice for 6 months. To track the biodistribution of ESC-sEVs in mice, DiR-labeled ESC-sEVs (1×10^{10} particles/mL, 100 μL) were injected into SAMP8 mice via tail vein injection, followed by euthanasia and *ex vivo* imaging of dissected organs 24 h after injection. As shown in Figure S4A, high intensity of fluorescent signals could be observed in the brain, heart, lung, liver, spleen, and kidneys. Meanwhile, no DiR signal was detected in naive SAMP8 mice. These results demonstrated the ability of ESC-sEVs to migrate into the brain and other organs in mice. We then investigated the anti-aging effects of ESC-sEVs in SAMP8 mice. As shown in Figure 2A, the escape latency was shorter while the duration in the target quadrant was much longer in the 12 month mice treated with ESC-sEVs than in the 12 month mice treated with PBS. Moreover, the decreased expression of hippocampal Syp, PSD-95, Gap-43, and Syn-IIa in 12 month mice was rescued by ESC-sEV treatment (Figure 2B). These data indicated that the application of ESC-sEVs could reverse cognitive deficits in aged mice. To investigate whether reversion of cognitive dysfunction in aging mice by ESC-sEVs was through ameliorating H-NSC senescence, we tested senescence-associated hallmarks in the hippocampus. As shown in Figure 2C, hippocampal SA-β-gal activity in 12 month mice treated with ESC-sEVs was much lower than in 12 month mice treated with PBS. The percentage of $Sox2^+/p16^{INK4a+}$ cells of total $Sox2^+$ cells in the SGZ also decreased in ESC-sEV-treated aged mice (Figure 2D). Subsequently, H-NSCs were isolated from the hippocampus and tested for senescence phenotypes. As shown in Figure 2E, the percentage of SA-β-gal^+ H-NSCs from ESC-sEV-treated aged mice was much lower than from PBS-treated aged mice. In addition, the expression levels of $p16^{INK4a}$, γ-H2AX, p21, and p53 proteins in the ESC-sEVs group were also reduced compared to the PBS group (Figure 2F). These results indicated that ESC-sEV treatment could decelerate the process of H-NSC senescence in mice during aging.

Furthermore, we detected the number of H-NSCs and immature neurons (DCX^+ cells) in the SGZ. As shown in Figures 3A and 3B, the number of $Sox2^+/Nestin^+$ cells and $Sox2^+/GFAP^+$ cells was much higher in ESC-sEV-treated mice than in PBS-treated mice. The number of proliferating H-NSCs ($Sox2^+/PCNA^+$ cells) was also increased in ESC-sEV-treated aged mice compared to PBS-treated aged mice (Figure 3C). Moreover, the number of DCX^+ cells and $DCX^+/PCNA^+$ cells was also markedly higher in ESC-sEV-treated mice than in PBS-treated mice (Figure 3D), which indicated that ESC-sEVs can promote hippocampal neurogenesis in aged mice. In addition, compared to H-NSCs isolated from PBS-treated mice, H-NSCs isolated from ESC-sEV-treated mice exhibited higher proliferation (Figures 3E and 3F) and neuronal differentiation (Figure 3G) abilities. Altogether, these results revealed that ESC-sEVs can restore the cognitive function of aged mice, and this effect may be mediated by rejuvenating the senescence of H-NSCs.

β-gal staining of the hippocampus and quantification of hippocampal SA-β-gal activity in 6 month, 12 month-PBS, and 12 month-sEV mice. Scale bars, 250 μm. n = 6 per group. ***p < 0.001. (D) IF images of senescent H-NSCs ($p16^{INK4a+}$, red; $Sox2^+$, green) and the percentage of $Sox2^+/p16^{INK4a+}$ double-stained cells in whole $Sox2^+$ cells in the SGZ of 6 month, 12 month-PBS, and 12 month-sEV mice. Scale bars, 50 μm. n = 6 per group. ***p < 0.001. (E) SA-β-gal staining of isolated H-NSCs and the percentage of SA-β-gal^+ cells in 6 month, 12 month-PBS, and 12 month-sEV mice. Scale bars, 100 μm. n = 6 per group. ***p < 0.001. (F) Western blot analysis and quantification of $p16^{INK4a}$, γ-H2AX, p21, and p53 in isolated neurospheres of 6 month, 12 month-PBS, and 12 month-sEV mice. n = 6 per group. ***p < 0.001.

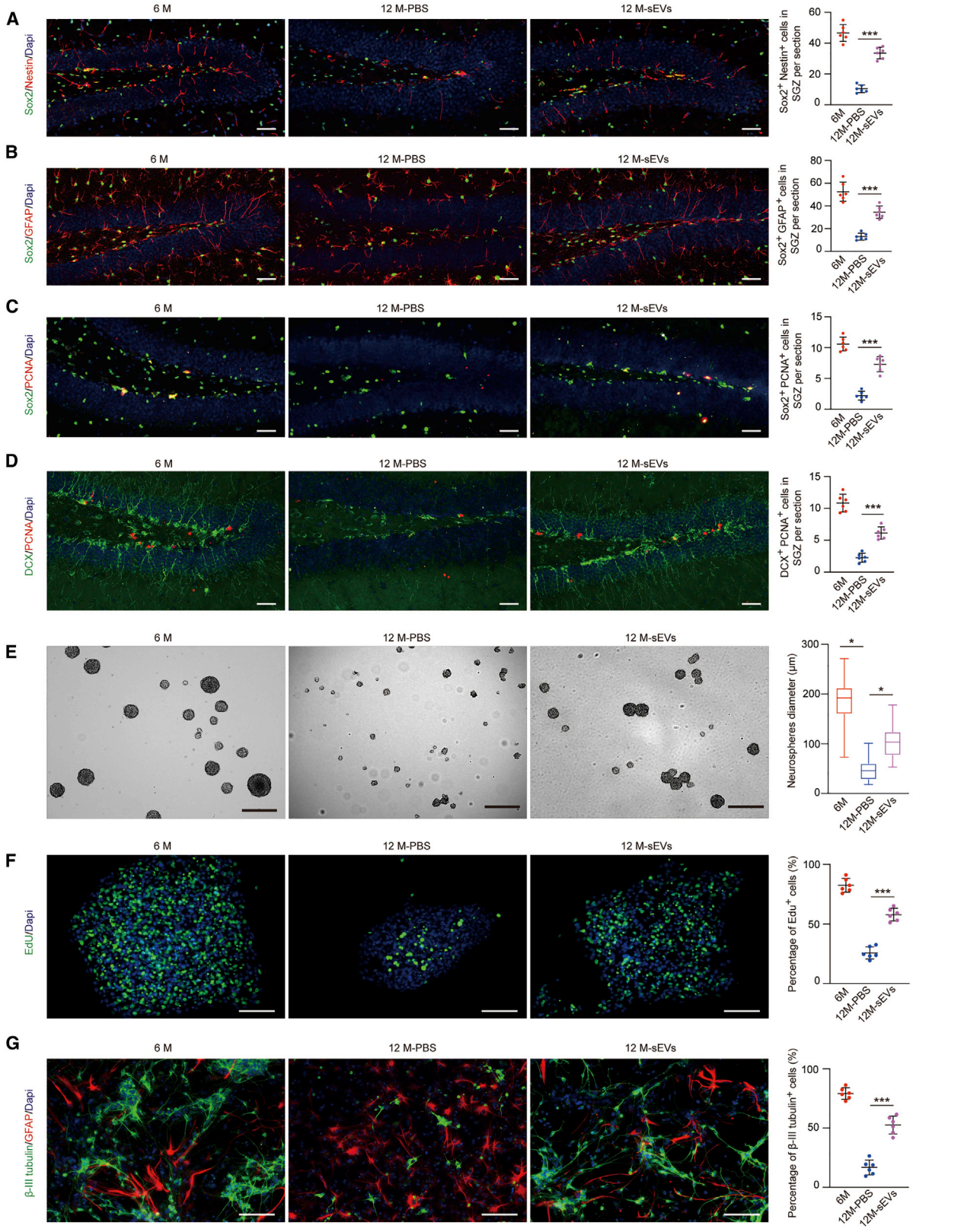

(legend on next page)

ESC-sEVs Rejuvenate Hippocampal NSC Senescence and Enhance NSC Activity *In Vitro*

The potential for self-renewal and differentiation in stem cells gradually decreases with continuous passaging, namely replicative senescence, which is regarded as an important *in vitro* model to explore stem cell function during aging.[25,26] In our study, we isolated H-NSCs from 2-week-old male C57BL/6 mice and applied the continuous passaging model to investigate the function and mechanism of ESC-sEVs in rejuvenating H-NSC senescence. Under culture conditions, primary H-NSCs can be passaged at most to passage 15, when the cells can hardly form neurospheres (Figure S5A). The neurospheres gradually decreased starting at passage 6 (Figures S5A and S5B). The Cell Counting Kit-8 (CCK8) assay also showed that the viability of H-NSCs before passage 6 is very high, gradually decreasing with passage number (Figure S5C). The SA-β-gal activity of H-NSCs from passage 2 to passage 6 is low and sharply increased with continuous passaging, reaching a plateau at passage 10 (Figure S5D). The expression level of $p16^{INK4a}$ in H-NSCs also reached the highest level at passage 10 (Figure S5E). Therefore, H-NSCs at passage 10 were used to test the effects of ESC-sEVs on senescence.

First, ESC-sEVs were labeled with DiO and cocultured with H-NSCs. We found that DiO-labeled ESC-sEVs can be internalized by H-NSCs (Figure S4B). Next, we applied ESC-sEVs to treat H-NSCs from passage 2 until passage 10. As shown in Figure 4A, ESC-sEV treatment reversed the increase of SA-β-gal activity in H-NSCs after continuous passaging. The expression level of $p16^{INK4a}$, γ-H2AX, p21, and p53 in H-NSCs was also decreased by the treatment with ESC-sEVs (Figure 4B). The application of ESC-sEVs also enhanced the proliferation and neuronal differentiation abilities of H-NSCs in passage 10 (Figures 4C–4E). These data further confirmed that H-NSC senescent phenotypes can be reversed by ESC-sEVs.

To elucidate the underlying mechanism involved in rejuvenating H-NSC senescence by ESC-sEVs, we performed RNA sequencing (RNA-seq) analysis to explore the change of gene expression in H-NSCs among passage 2 (NSCs-P2), passage 10 treated with ESC-sEVs (1×10^{10} particles/mL ESC-sEVs treated from passage 2 to passage 10 [NSCs-P10-sEVs]), and passage 10 treated with PBS (the same amount of PBS treated from passage 2 to passage 10 [NSCs-P10-PBS]), and the results were listed in Data S1. We applied the "Calculate and draw custom Venn diagrams" online tool (http://bioinformatics.psb.ugent.be/webtools/Venn/) to identify the significantly upregulated or downregulated genes across NSCs-P2 against NSCs-P10-PBS, as well as NSCs-P10-sEVs against NSCs-P10-PBS, and selected the co-upregulated or co-downregulated genes between NSCs-P2 against NSCs-P10-PBS and NSCs-P10-sEVs against NSCs-P10-PBS. As shown in Figure 4F, we identified 232 co-upregulated genes (>1.5-fold, $p < 0.05$) and 415 co-downregulated genes (< 0.75-fold, $p < 0.05$). Among them, 23 genes (10 genes were co-upregulated and 13 genes were co-downregulated) were involved in the nervous system and were selected as candidate genes that may function in regulating NSC senescence (Figures S6A and S6B). qRT-PCR was used to verify the expression level of these genes (Figures S6C and S6D). MYT1 is expressed in differentiating progenitors and postmitotic neuronal precursors of the central nervous system and peripheral nervous system, and it has been demonstrated to regulate neurogenesis in mice.[27,28] Our RNA-seq analysis as well as later qRT-PCR and western blot showed that MYT1 is highly expressed in H-NSCs at passage 2 and significantly downregulated at passage 10, while coculture with ESC-sEVs upregulated MYT1 expression in H-NSCs at passage 10 (Figures 4G and 4H). The expression level of MYT1 in H-NSCs isolated from 2 month, 6 month, and 12 month SAMP8 mice was also gradually decreased, while the application of ESC-sEVs significantly increased MYT1 expression in the H-NSCs of 12 month mice when compared to PBS-treated 12 month mice (Figure 4I). Therefore, we supposed that MYT1 may possess a potential role in regulating H-NSC senescence to influence neurogenesis, and ESC-sEVs rejuvenated H-NSC senescence in aged mice likely via upregulation of MYT1.

ESC-sEVs Rejuvenate Senescent Hippocampal NSCs by Upregulating MYT1

To address whether MYT1 is involved in regulating H-NSC senescence, we generated young H-NSCs (passage 2 from 2-week-old male C57BL/6 mice) with constitutive knockdown of either a MYT1 transgene (short hairpin RNA [shRNA] [sh]-MYT1) or a GFP control transgene (sh-negative control [sh-NC]) and identified their senescent phenotype. qRT-PCR and western blot showed the downregulation of MYT1 at both the RNA and protein level, and sh-MYT1 showed the highest efficiency and was chosen for the following experiments (Figures 5A and 5B). SA-β-gal staining (Figure S7A) and western blot for $p16^{INK4a}$ and γ-H2AX (Figure S7B) showed an increase of the senescent phenotype in H-NSCs after MYT1 knockdown. The diameter of sh-NC neurospheres was larger

Figure 3. ESC-sEVs Reverse H-NSC Depletion and Promote Neurogenesis in the SGZ of SAMP8 Mice

(A) IF images for hippocampal $Sox2^+$ (green) and $Nestin^+$ (red) cells and the number of $Sox2^+/Nestin^+$ double-stained cells in the SGZ of 6 month, 12 month-PBS, and 12 month-sEV mice. Scale bars, 50 μm. n = 6 per group. ***$p < 0.001$. (B) IF images for hippocampal $Sox2^+$ (green) and $GFAP^+$ (red) cells and the number of $Sox2^+/GFAP^+$ double-stained cells in the SGZ of 6 month, 12 month-PBS, and 12 month-sEV mice. Scale bars, 50 μm. n = 6 per group. ***$p < 0.001$. (C) IF images for proliferated H-NSCs ($Sox2^+$, green; $PCNA^+$, red) and the number of $Sox2^+/PCNA^+$ double-stained cells in the SGZ of 6 month, 12 month-PBS, and 12 month-sEV mice. Scale bars, 50 μm. n = 6 per group. ***$p < 0.001$. (D) IF images for hippocampal DCX^+ (green) and $PCNA^+$ (red) cells and the number of $DCX^+/PCNA^+$ double-stained cells in the SGZ of 6 month, 12 month-PBS, and 12 month-sEV mice. Scale bars, 50 μm. n = 6 per group. ***$p < 0.001$. (E) Neurosphere formation and quantification of neurosphere diameters in 6 month, 12 month-PBS, and 12 month-sEV mice. Scale bars, 300 μm. n = 6 per group. *$p < 0.05$. (F) IF images for EdU incorporation in isolated neurospheres and the percentage of $EdU^+/DAPI^+$ double-stained cells from total $DAPI^+$ cells in 6 month, 12 month-PBS, and 12 month-sEV mice. Scale bars, 100 μm. n = 6 per group. ***$p < 0.001$. (G) IF images for β-tubulin III^+ (green) and $GFAP^+$ cells and the percentage of β-tubulin III^+ cells in whole cells in 6 month, 12 month-PBS, 12 month-ESC-sEV mice. Scale bars, 100 μm. n = 6 per group. ***$p < 0.001$.

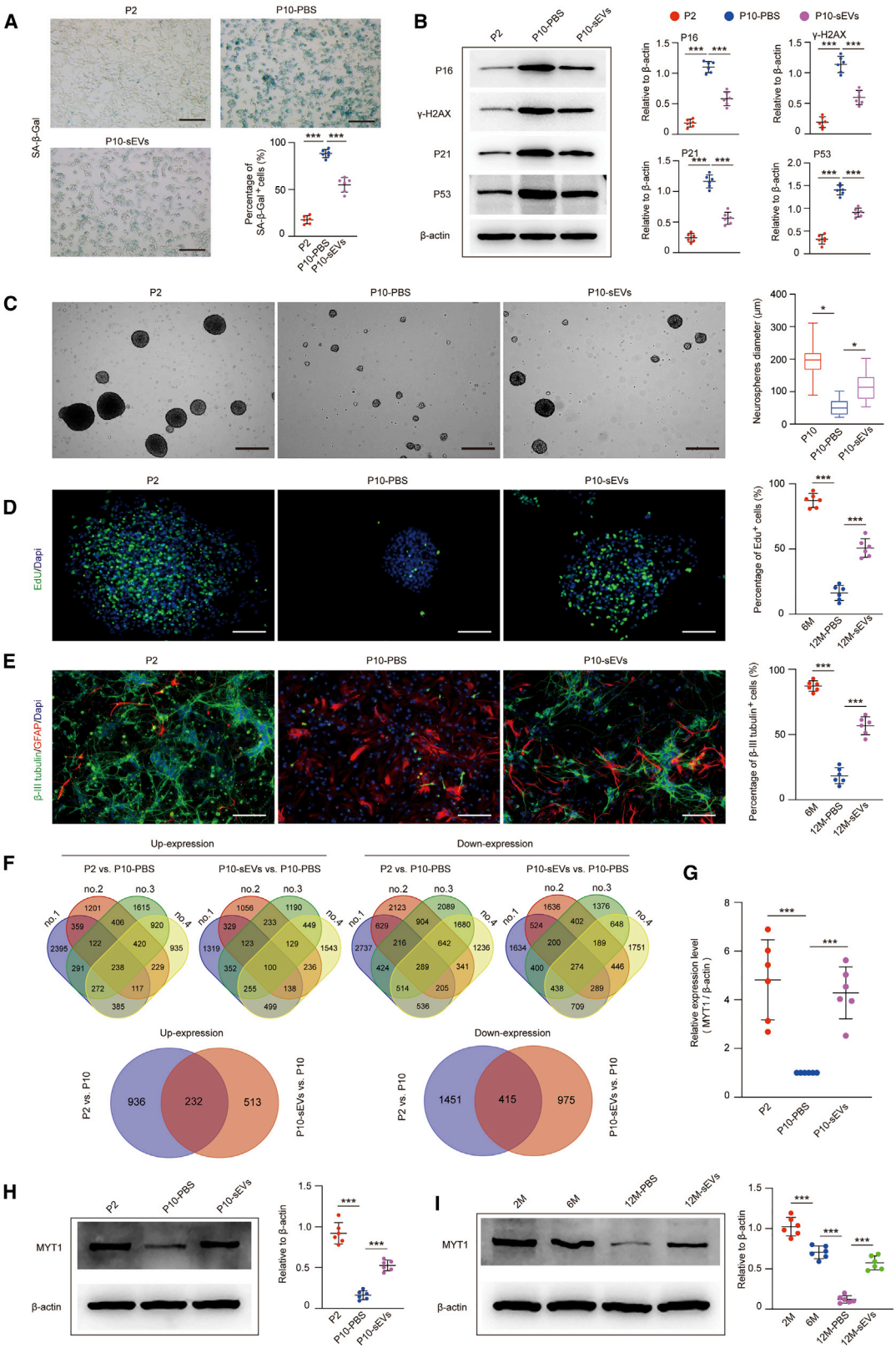

(legend on next page)

(Figure S7C), and the percentage of differentiated neurons was higher (Figure S7D) than that of the sh-MYT1 group. These results suggested that downregulation of MYT1 levels may induce senescence and reduce the proliferation and neuronal differentiation capacity of H-NSCs.

To further determine whether MYT1 is a crucial factor for the anti-senescence effect of ESC-sEVs on H-NSCs, we applied ESC-sEVs or PBS to treat sh-MYT1 NSCs and sh-NC NSCs for three passages (passage 3 to passage 5). As shown in Figures 5C and 5D, ESC-sEV treatment reduced SA-β-gal activity and the expression of $p16^{INK4a}$, γ-H2AX, p21, and p53 in H-NSCs after passaging, while knockdown of MYT1 abolished the downregulation effects of ESC-sEVs on the activity of SA-β-gal and the expression of $p16^{INK4a}$, γ-H2AX, p21, and p53. In addition, knockdown of MYT1 also resulted in the functional impairment of ESC-sEVs in promoting H-NSC self-renewal and neurogenesis (Figures 5E–5G). Taken together, these results confirmed that MYT1 was involved in the regulation of H-NSC senescence, and ESC-sEVs rejuvenated senescent H-NSCs and promoted their proliferation as well as neuronal differentiation partly by the upregulation of MYT1.

ESC-sEVs Rejuvenate Senescent Hippocampal NSCs by Regulating the MYT1-Egln3-Sirt1 Axis

We further investigated the mechanism of how MYT1 regulates H-NSC senescence. Vasconcelos et al.[28] performed transcriptome sequencing for neural stem cell line NS5 with MYT1 overexpression, and they identified 1,002 downregulated genes and 761 upregulated genes. By analyzing these data with our RNA-seq results, we selected four upregulated genes (Pou5f2, Pcdhga11, Pde5a, and Tspan2) and nine downregulated genes (Dusp6, Wls, Il33, Kif21a, Pcdhb5, S100b, Frk, Egln3, and Abca9) (Figure S8A). qRT-PCR showed that Egln3 was significantly upregulated in sh-MYT1 NSCs compared with that in sh-NC NSCs (Figure S8B). Western blot also confirmed the results at the protein level (Figure S8C). These results indicated that MYT1 can inhibit Egln3 in H-NSCs.

Egln3 (also known as PHD3) encodes an intracellular prolyl hydroxylase that is involved in the cellular response to oxygen availability by stabilizing HIF-2α.[29] Moreover, it has been demonstrated that HIF-2α can directly target NAMPT (also known as visfatin) and positively regulate the expression of NAMPT,[30] which is involved in the amelioration of senescence via upregulation of Sirt1.[31,32] In our study, we found that the expression levels of HIF-2α, NAMPT, and Sirt1 were decreased significantly in sh-MYT1 NSCs compared with sh-NC NSCs (Figure S8D). These results confirmed that MYT1 may inhibit Egln3 and promote the expression of its downstream molecules, including HIF-2α, NAMPT, and Sirt1 in H-NSCs. Furthermore, we showed that ESC-sEV treatment reduced the expression of Egln3 and increased the expression of HIF-2α, NAMPT, and Sirt1, while knockdown of MYT1 impaired these effects of ESC-sEVs (Figure 6A). These results indicated that MYT1 mediated the effects of ESC-sEVs on the expression of Egln3 and its downstream molecules in H-NSCs.

ESC-sEVs Ameliorate Hippocampal NSC Senescence by Transferring SMADs to Regulate the MYT1-Egln3-Sirt1 Axis

Encapsulated proteins are one of the key molecules in sEVs that modulate recipient cell function.[33] From our previous liquid chromatography-tandem mass spectrometry (LC-MS/MS) data identifying the protein content in ESC-sEVs (ProteomeXchange Consortium dataset identifier PXD018655),[34] we found 4,122 proteins in ESC-sEVs, and 3,686 proteins can be aligned to the EV proteome database Vesiclepedia (Figure 6B). Cellular component analysis by Gene Ontology (GO) analysis also showed that most of the proteins belonged to the EVs (Figure 6C). Sherry-Lynes et al.[35] had suggested that bone morphogenetic proteins (BMPs) can activate the SMAD signaling cascade to upregulate the expression of Myt1. As LC-MS/MS analysis had identified that SMAD4 and SMAD5 were encapsulated in ESC-sEVs, western blot also confirmed the enrichment of SMAD4 and SMAD5 in ESC-sEVs (Figure 6D), and the expression of SMAD4, SMAD5, and phosphorylated SMAD5 (p-SMAD5) were enhanced in H-NSCs when treated by ESC-sEVs (Figure 6E). Thus, we supposed that ESC-sEVs may transfer SMAD4 and SMAD5 to upregulate MYT1 in H-NSCs.

As shown in Figure 6F, compared with the control group, H-NSCs treated with recombinant BMP4 (25 ng/mL, PeproTech) for 6 h exhibited higher expression of p-SMAD5, SMAD4, and MYT1, while treatment with LDN-193189 (LDN, 200 nM, Selleck Chemicals) for 30 min significantly inhibited the expression of p-SMAD5, SMAD4, and MYT1, which were hardly reversed by treatment with BMP4 for 6 h. These results indicated that MYT1 activation was associated

Figure 4. ESC-sEVs Upregulate MYT1 in H-NSCs and Ameliorate H-NSC Senescence

(A) Representative images of SA-β-gal staining and the percentage of SA-β-gal^+ cells in passage 2 (P2) H-NSCs, passage 10 H-NSCs treated with PBS (P10-PBS), and passage 10 H-NSCs treated with ESC-sEVs (P10-sEVs). Scale bars, 100 μm. n = 6 per group. ***$p < 0.001$. (B) Western blot analysis and quantification of $p16^{INK4a}$, γ-H2AX, p21, and p53 in H-NSCs of P2, P10-PBS, and P10-sEVs. n = 6 per group. ***$p < 0.001$. (C) Neurosphere formation and quantification of neurosphere diameters in H-NSCs of P2, P10-PBS, and P10-sEVs. Scale bars, 300 μm. n = 6 per group. *$p < 0.05$. (D) IF images for EdU incorporation in neurospheres and the percentage of EdU^+/$DAPI^+$ double-stained cells in whole $DAPI^+$ cells in H-NSCs of P2, P10-PBS, and P10-sEVs. Scale bars, 100 μm. n = 6 per group. ***$p < 0.001$. (E) IF images for β-tubulin III^+ (green) and $GFAP^+$ cells and the percentage of β-tubulin III^+ cells in whole cells in H-NSCs of P2, P10-PBS, and P10-sEVs. Scale bars, 100 μm. n = 6 per group. ***$p < 0.001$. (F) RNA-seq data from H-NSCs of P2, P10-PBS, and P10-sEVs were analyzed by the "Calculate and draw custom Venn diagrams" online tool; 232 genes were co-upregulated and 415 genes were co-downregulated in P2 versus P10-PBS and P10-sEVs versus P10-PBS. n = 4 per group. (G) The relative expression level of MYT1 in H-NSCs of P2, P10-PBS, and P10-sEVs was detected by qRT-PCR. n = 6 per group. ***$p < 0.001$. (H) Western blot analysis and quantification of MYT1 in H-NSCs of P2, P10-PBS, and P10-sEVs. n = 6 per group. ***$p < 0.001$. (I) Western blot analysis and quantification of MYT1 in isolated neurospheres of 2 month, 6 month, and 12 month-PBS and 12 month-sEV mice. n = 6 per group. ***$p < 0.001$.

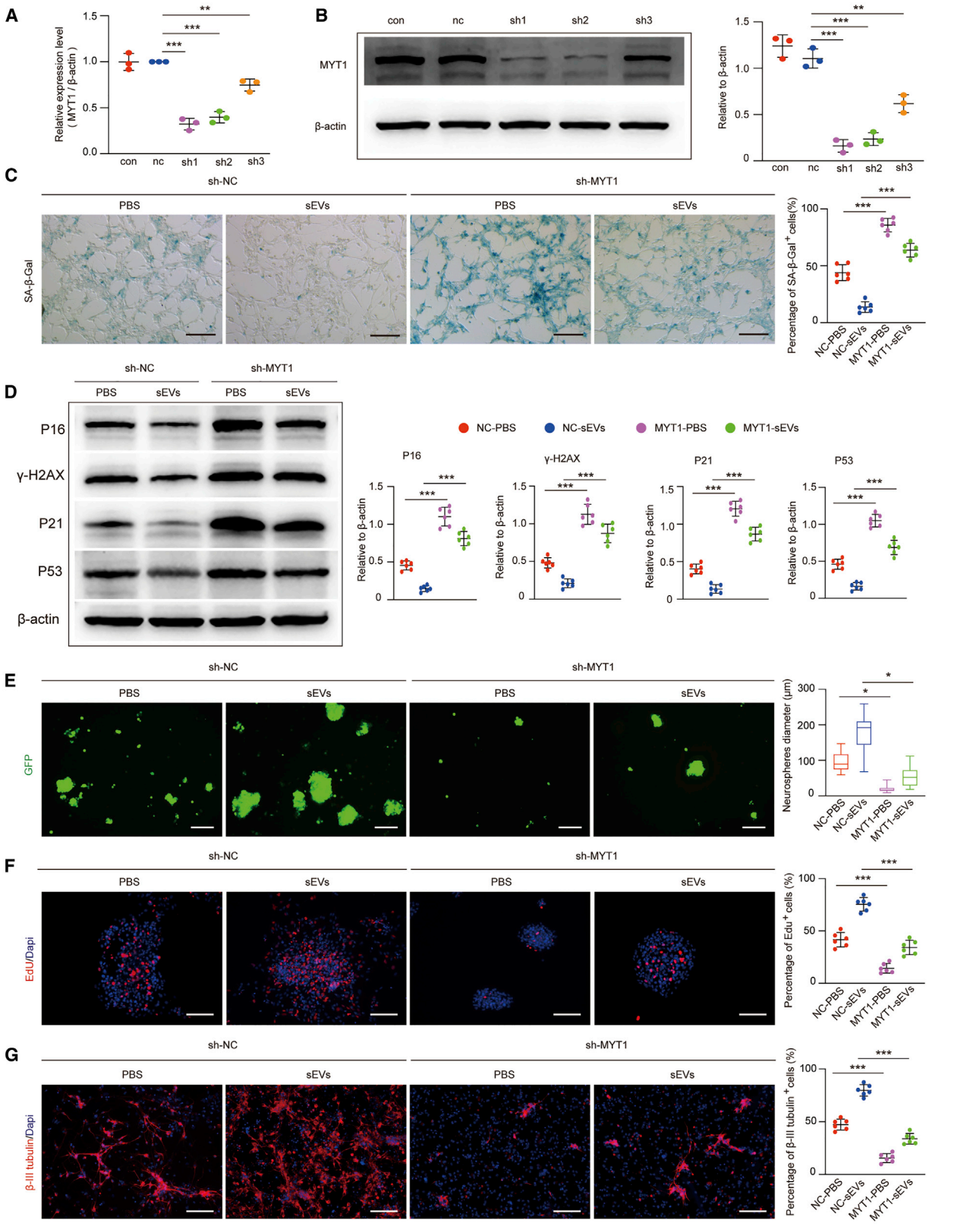

(legend on next page)

with the activation of SMAD4 and SMAD5 in H-NSCs. We further detected the expression of these proteins in H-NSCs from a replicative senescence model and SAMP8 mice. The protein levels of p-SMAD5, SMAD5, SMAD4, MYT1, HIF-2α, NAMPT, and Sirt1 were decreased and Egln3 was activated after continuous passaging of H-NSCs, while this tendency was reversed after treatment with ESC-sEVs (Figure S9). In addition, the date from isolated H-NSCs of SAMP8 mice also confirmed the decreasing tendency of p-SMAD5, SMAD4, MYT1, HIF-2α, NAMPT, and Sirt1 and the increasing tendency of Egln3, as well as the function of ESC-sEVs in reversion of the expression tendency of these proteins (Figure 6G).

In addition, the anti-senescence effects of ESC-sEVs were further confirmed using C57BL/6 mice by intravenous injection into 12-month-old mice for 8 months. As shown in Figure 7A, the escape latency was shorter while the duration in the target quadrant was much longer in 20 month mice treated with ESC-sEVs than in 20 month mice treated with PBS. The expression of hippocampal Syp, PSD-95, Gap-43, and Syn-IIa in 20 month mice was also enhanced by ESC-sEVs (Figure 7B). Inconsistent with the results from SAMP8 mice, these results indicated that ESC-sEVs can also reverse cognitive dysfunction of natural aged C57BL/6 mice. Western blot showed that the protein levels of p-SMAD5, SMAD5, SMAD4, MYT1, HIF-2α, NAMPT, and Sirt1 were increased, while Egln3 was decreased, in H-NSCs isolated from ESC-sEV-treated C57BL/6 mice (Figure 7C). In addition, hippocampal SA-β-gal activity and the percentage of $Sox2^{+}/p16^{INK4a+}$ cells from the total $Sox2^{+}$ cells in the SGZ were decreased in ESC-sEV-treated aged C57BL/6 mice (Figures 7D and 7E). The percentage of SA-β-gal^{+} H-NSCs and the expression levels of $p16^{INK4a}$, γ-H2AX, p21, and p53 in H-NSCs were also reduced from ESC-sEV-treated C57BL/6 mice (Figures 7F and 7G). Additionally, the number of $Sox2^{+}$/$GFAP^{+}$ cells and $Sox2^{+}$/5-ethynyl-2′-deoxyuridine $(EdU)^{+}$ cells were found to be significantly higher in ESC-sEV-treated C57BL/6 mice than in PBS-treated mice (Figures 7H and 7I). Taken together, these results demonstrated that ESC-sEVs can transfer SMAD4 and SMAD5 to upregulate MYT1 in H-NSCs, and then inhibit Egln3 and promote HIF-2α, NAMPT and Sirt1 expression, which resulted in senescent H-NSC rejuvenation, as well as self-renewal and neurogenesis recovery, followed by cognitive recovery.

DISCUSSION

Stem cells exhibited senescence phenotypes in many tissues with the advance of aging. These senescent stem cells showed similar features, such as blunted responsiveness to tissue injury and dysregulation of proliferation, differentiation, and function, which resulted in the reduction of effective cellular replacement and tissue regeneration in aged organisms.[36,37] Accordingly, therapeutic strategies, including cellular reprogramming,[38] stem cell transplantation,[39] and senolytics (i.e., ABT263),[40] have been demonstrated to effectively rejuvenate or eliminate senescent tissue-specific stem cells to promote functional recovery. Research on stem cell aging and anti-aging suggested that senescent stem cells were important pathogenesis as well as therapeutic targets for age-related diseases. In this study, we reported that H-NSC senescence is accompanied with the progress of aging. In accordance with other studies,[9–11] senescent H-NSCs exhibited significant senescent phenotypes with impairment of proliferation and neuronal differentiation capacities, which partly caused the aging-related decline of H-NSCs and neurogenesis in the hippocampus.[23]

Stem cell-derived sEVs have been reported to have therapeutic potential in the treatment of diseases from various organs, including the brain,[41] heart,[14] and kidney,[42] which indicated that sEVs derived from stem cells hold great potential in regenerative medicine. Recent evidence has demonstrated that ESC-sEVs possess the ability to promote tissue recovery via amelioration of somatic cell senescence.[18,19] However, whether ESC-sEVs could rejuvenate aging-related senescent H-NSCs and restore their capacity is still unknown. In our study, we found that chronic application of ESC-sEVs could markedly reduce the senescence hallmarks, recover the compromised self-renewal and neurogenesis capacity of H-NSCs, and result in cognitive recovery in mice during aging. Our study suggested that ESC-sEVs can rejuvenate age-related senescence in H-NSCs and thereby reverse cognitive dysfunction with aging.

We further applied RNA-seq to identify the intrinsic changes of H-NSCs in a replicative senescence model. Hundreds of genes could be candidate regulators of H-NSC aging as well as the target for ESC-sEVs to rejuvenate senescence. As an initial step, we identified MYT1 as a putative age-associated regulator of H-NSC senescence and functional decline. MYT1 was downregulated in senescent H-NSCs, and knockdown of MYT1 in young H-NSCs promoted aging-related phenotypes, including an increase of SA-β-gal activity and the expression of $p16^{INK4a}$, γ-H2AX, p21, p53, and the reduction of proliferation and neuronal differentiation abilities. Furthermore, we identified that Egln3, which was found to be increased in aged mouse and human hearts[43] and upregulated in senescent H-NSCs,

Figure 5. Knockdown of MYT1 Accelerates H-NSC Senescence and Abolishes the Anti-aging Function of ESC-sEVs

(A) The knockdown efficiency of MYT1 shRNAs in H-NSCs was detected by qRT-PCR. n = 3 per group. $^{**}p < 0.01$, $^{***}p < 0.001$. (B) Western blot analysis and quantification of MYT1 in H-NSCs showing the knockdown efficiency of MYT1 shRNAs. n = 3 per group. $^{**}p < 0.01$, $^{***}p < 0.001$. (C) SA-β-gal staining and the percentage of SA-β-gal^{+} cells in sh-NC NSCs treated with PBS or ESC-sEVs (sh-NC-PBS or sh-NC-sEVs) and sh-MYT1 NSCs treated with PBS or ESC-sEVs (sh-MYT1-PBS or sh-MYT1-sEVs). Scale bars, 100 μm. n = 6 per group. $^{***}p < 0.001$. (D) Western blot analysis and quantification of $p16^{INK4a}$, γ-H2AX, p21, and p53 in H-NSCs of sh-NC-PBS, sh-NC-sEVs, sh-MYT1-PBS, and sh-MYT1-sEVs. n = 6 per group. $^{***}p < 0.001$. (E) IF images for GFP-labeled neurospheres and the diameter of neurospheres in H-NSCs of sh-NC-PBS, sh-NC-sEVs, sh-MYT1-PBS, and sh-MYT1-sEVs. Scale bars, 200 μm. n = 6 per group. $^{*}p < 0.05$. (F) IF images for EdU incorporation in neurospheres and the percentage of EdU^{+}/$DAPI^{+}$ double-stained cells in all $DAPI^{+}$ cells in sh-NC-PBS, sh-NC-sEVs, sh-MYT1-PBS, and sh-MYT1-sEVs. Scale bars, 100 μm. n = 6 per group. $^{***}p < 0.001$. (G) IF images for β-tubulin III^{+} and the percentage of β-tubulin III^{+} cells in whole cells in H-NSCs of sh-NC-PBS, sh-NC-sEVs, sh-MYT1-PBS, and sh-MYT1-sEVs. Scale bars, 100 μm. n = 6 per group. $^{***}p < 0.001$.

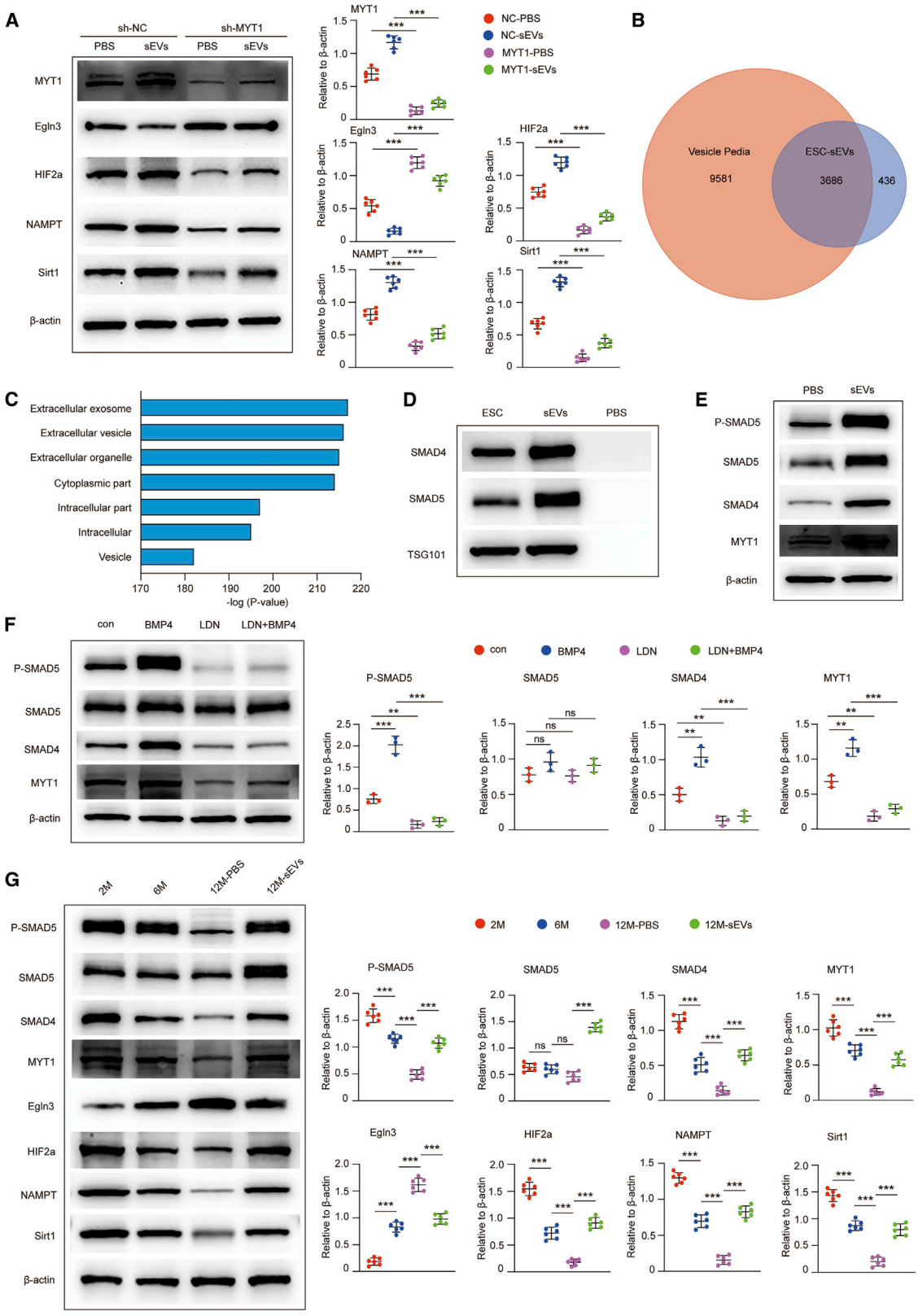

(legend on next page)

is negatively regulated by MYT1, because knockdown of MYT1 expression in young H-NSCs significantly increased the expression level of Egln3. Egln3 encodes intracellular prolyl hydroxylase that regulates HIF-α expression,[44] and it has been demonstrated to mainly regulate the expression of HIF-2α.[29] Meanwhile, HIF-2α can directly target NAMPT, and it positively regulates the expression of NAMPT,[30] which ameliorates senescence via upregulation of Sirt1.[31,32] In addition, NAMPT and Sirt1 are important regulators involved in NSC maintenance. NAMPT is the main source of nicotinamide adenine dinucleotide $(NAD)^+$ and is required for G_1/S progression in NSCs. Stein and Imai[45] revealed that the expression level of NAD^+ and NAMPT decreased with age in the hippocampus. The adult NSC pool was significantly exhausted *in vivo* when NAMPT was ablated during aging, while it can be rescued by enhancing hippocampal NAMPT levels. Sirt1 can positively modulate the Wnt signaling pathway,[46] which plays the key role in the regulation of NSC homeostasis during development and in the adult brain. Additionally, genes and proteins involved in Wnt/β-catenin signaling within the SVZ and the SGZ niches were markedly downregulated in aging, inflammation/oxidative stress, and neurodegeneration diseases, while most of the neurogenesis-promoting factors (including Sirt1, BMP/SMAD, and HIF-α) or treatments that reverse neurogenesis downregulation act, at least in part, in cooperation/synergy with Wnt/β-catenin signaling intermediacy.[47–49] In our study, we found that HIF-2α, NAMPT, and Sirt1 were downregulated in senescent H-NSCs as well as in MYT1 knockdown of young H-NSCs. In addition, ESC-sEV treatment significantly rescued the decrease of MYT1, HIF-2α, NAMPT, and Sirt1, and it reversed the increase of Egln3 in senescent H-NSCs, while this function was abolished by the knockdown of MYT1. Taken together, these data suggested that the therapeutic effect of ESC-sEVs in rejuvenating H-NSC senescence was partly attributed to upregulation of MYT1 to inhibit Egln3, improving the expression of HIF-2α, NAMPT, and Sirt1.

Recently, many studies have demonstrated that sEVs acted as a delivery system partly by transferring their proteins to recipient cells to alter their gene expression and bioactivity.[50,51] For example, Rong et al.[50] revealed that NSC-sEVs could deliver 14-3-3t protein to interact with Beclin-1 to activate autophagy in injured spinal cords, and they promoted their functional behavior recovery. Therefore, we hypothesized that ESC-sEVs ameliorate H-NSC senescence by delivering functional proteins to upregulate MYT1 in senescent H-NSCs during aging. In our LC-MS/MS data,[34] 4,122 proteins were identified from ESC-sEVs, and 3,686 proteins were aligned to the EV proteome database EVpedia, and most of the proteins belonged to the EVs. It has been previously reported that activation of the SMAD signaling cascade can upregulate the expression of MYT1.[35] Generally, the activation of the SMAD pathway can be defined as phosphorylation of the C terminus of SMAD1, SMAD5, or SMAD8, leading to the formation of a complex with SMAD4 and translocating into the nucleus to regulate the expression of specific genes.[52] As activation of the SMAD signaling cascade can also promote neurogenesis,[53] we then identified whether ESC-sEVs transfer SMADs to regulate MYT1 in H-NSCs. In our study, we found that SMAD4 and SMAD5 are highly enriched in ESC-sEVs, and they can be delivered into H-NSCs to improve the expression levels of SMAD4, SMAD5, and p-SMAD5. We further detected the relationship between SMAD4, SMAD5, and MYT1 in H-NSCs, and we demonstrated that activation of SMAD4 and p-SMAD5 can upregulate MYT1 in H-NSCs. Collectively, our study reveals a close link between proteins enriched in ESC-sEVs and the anti-aging genes in H-NSCs, and it highlights the critical role of SMAD4 and SMAD5 in ESC-sEVs to positively regulate MYT1 to reverse the senescence of H-NSCs. However, as sEVs are complex "living" structures that encapsulate proteins, trophic factors, miRNAs, and RNAs are important molecules in sEVs to modulate recipient cell function.[51,54] Previous studies have demonstrated that ESC-sEVs can transfer highly enriched miR-200a to ameliorate endothelial senescence.[19] In our study, we found that MYT1 knockdown cannot totally reverse the anti-senescence function of ESC-sEVs. Therefore, taken together, we think that other mechanisms, including encapsulation of miRNAs in ESC-sEVs, can also function to rejuvenate H-NSC senescence.

Furthermore, neurons, astrocytes, oligodendrocytes, vasculature, extracellular matrix and associated molecules, and structural elements and molecules in NSC niches are important in supporting the lifelong self-renewal of NSCs and the production of differentiated cells.[55] The alteration of structural elements (such as inflammation) during aging plays a crucial role in inducing NSC senescence, dysfunction, and exhaustion. For example, Yousef et al.[56] demonstrated that the blood-brain barrier was damaged, microglia were activated, and inflammatory cytokines (tumor necrosis factor [TNF]-α, interleukin [IL]-1β, and IL-6) were overexpressed in the aged hippocampus, which can cause H-NSC exhaustion and neurogenesis reduction. Notch1 signaling downregulation in the NSC niche of the aged brain also results in NSC loss and neurogenesis reduction.[57] Our *in vivo* results in Figures 2C and 2D show that the hippocampal SA-β-gal activity and the $p16^{INK4a}$ fluorescence intensity of

Figure 6. ESC-sEVs Rejuvenate Senescent H-NSCs by Transferring SMADs to Activate MYT1, Inhibit Egln3, and Upregulate HIF-2α, NAMPT, and Sirt1 Successively

(A) Western blot analysis and quantification of MYT1, Egln3, HIF-2α, NAMPT, and Sirt1 in H-NSCs of sh-NC-PBS, sh-NC-sEVs, sh-MYT1-PBS, and sh-MYT1-sEVs. n = 6 per group. ***p < 0.001. (B) Comparison of proteins in ESC-sEVs identified by LC-MS/MS with the EV proteome database Vesiclepedia. (C) GO analysis of proteins in ESC-sEVs showed mostly that proteins belonged to extracellular vesicles. (D) Western blot analysis of SMAD4, SMAD5, and TSG101 in ESCs, ESC-sEVs, and PBS. (E) Western blot analysis and quantification of p-SMAD5, SMAD5, SMAD4, and MYT1 in H-NSCs treated with PBS and ESC-sEVs. (F) Western blot analysis and quantification of p-SMAD5, SMAD5, SMAD4, and MYT1 in H-NSCs, H-NSCs treated with 25 ng/mL BMP4, H-NSCs treated with 200 nM LDN-193189, and H-NSCs treated with LDN-193189 and BMP4. n = 3 per group. **p < 0.01, ***p < 0.001. (G) Western blot analysis and quantification of p-SMAD5, SMAD5, SMAD4, MYT1, Egln3, HIF-2α, NAMPT, and Sirt1 in isolated neurospheres of 2 month, 6 month, and 12 month-PBS and 12 month-sEV mice. n = 6 per group. ***p < 0.001.

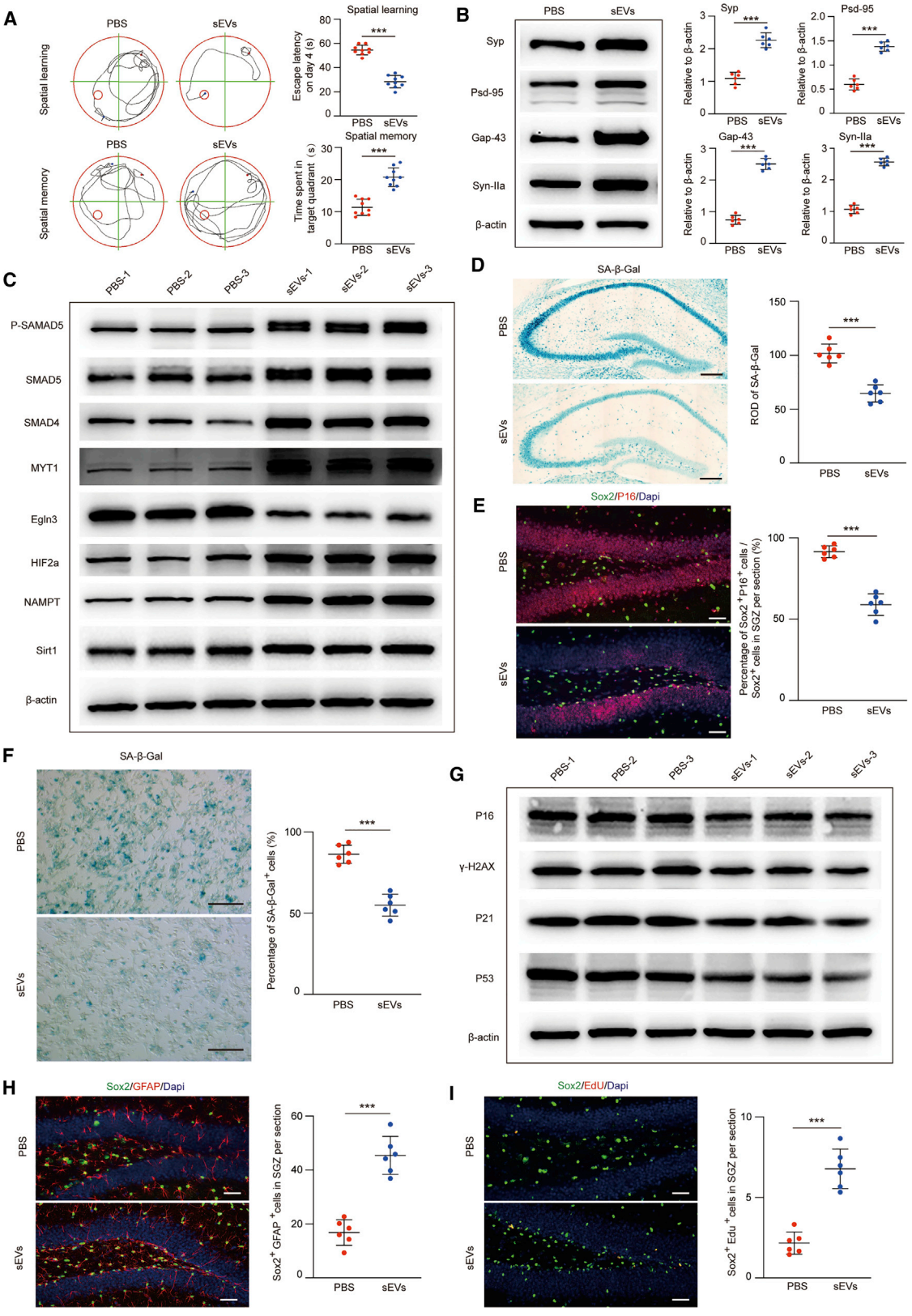

(legend on next page)

hippocampus in 12 month SAMP8 mice treated with ESC-sEVs was much lower than 12 month mice treated with PBS, indicating that ESC-sEV treatment could also improve the senescent status of non-NSCs in hippocampus, suggesting that the microenvironment in the NSC niches was switched toward youth by the ESC-sEV treatment. Thus, ESC-sEVs may also modify the microenvironment in the NSC niche to rejuvenate H-NSCs, and this still needs further investigation.

In summary, our data demonstrated that the downregulation of MYT1 in H-NSCs during aging can induce cell senescence, which impairs their proliferation and neuronal differentiation capacities, and may be one of the factors that results in H-NSC exhaustion, neurogenesis reduction, and cognitive impairment. ESC-sEVs exhibited a positive effect on rejuvenating H-NSC senescence partly by transferring their highly enriched SMAD4 and SMAD5 to activate MYT1, inhibit Egln3, and increase the expression of HIF-2α, NAMPT, and Sirt1 successively. Thus, these findings highlight a novel cell-free therapeutic tool for rejuvenating senescent resident stem cells to treat age-related diseases.

MATERIALS AND METHODS

Details of the materials and experimental procedures are available in the Supplemental Information, and the models and methods used for each *in vivo*/*ex vivo*/*in vitro* study are summarized in Table S3. The data that support the findings of this study are available from the corresponding authors on reasonable request.

ESC Culture and ESC-sEV Isolation and Identification

The human ESCs (H9) were provided by the Institute of Biochemistry and Cell Biology of Chinese Academy of Sciences, and they were cultured in ncEpic hPSC medium (Nuwacell Biotechnologies). ESC-sEVs were isolated by differential centrifugation/ultracentrifugation protocols and identified by TEM, nano-flow cytometry, and western blot. Further details are provided in the Supplemental Information.

Animal Experimental Procedures

Animal care and experimental procedures were approved by the Animal Research Committee of the Shanghai Jiao Tong University Affiliated Sixth People's Hospital (approval code: DWSY2018-118). Male SAMP8 mice and male C57BL/6 mice were housed under pathogen-free conditions and provided a standard diet and water. For the *in vivo* study, mice were treated with 100 μL of PBS or ESC-sEVs (1×10^{10} particles dissolved in 100 μL of PBS) by tail vein injection twice weekly. 6-month-old male SAMP8 mice were treated for 6 months until sacrifice at 12 months of age, and 12-month-old male C57BL/6 mice were treated for 8 months until sacrifice at 20 months of age. C57BL/6 mice were injected with EdU (50 mg/kg per mouse) 5, 3, and 1 days before sacrifice to label the proliferated cells.

H-NSC Isolation and Culture, and the Effects of ESC-sEVs on H-NSC Senescence, Proliferation, and Differentiation

H-NSCs were isolated from the hippocampus of mice and cultured in complete NSC medium as described previously.[58] Briefly, H-NSCs were incubated with 1×10^{10} particles/mL ESC-sEVs or an equal volume of PBS from passage 2 to passage 10. Then, neurospheres were collected for experiments including SA-β-gal staining and western blot. For the Edu incorporation assay, neurospheres were dissociated and 20,000 cells were incubated in complete NSC medium for 4 days, and then EdU (10 μM) was added to culture medium for 4 h. Next, neurospheres were fixed with 4% paraformaldehyde (PFA), and immunofluorescence (IF) staining with EdU and DAPI was used to evaluate cell proliferation (percentage of EdU^+ cells in total cells). For the differentiation assay, neurospheres were dissociated and 50,000 cells were plated on poly-L-lysine-coated 48-well plates. Cells were cultured with the differentiation medium for 5 days. Next, cells were fixed and IF double staining of β-tubulin III and GFAP were applied to calculate the percentage of $\beta\text{-tubulin III}^+$ cells in total cells. Further details are provided in the Supplemental Information.

SA-β-gal Staining

SA-β-gal staining of brain sections and cultured NSCs was performed using an SA-β-gal staining kit. The activity of SA-β-gal for hippocampus in brain sections was evaluated by means of the ROD (relative optical density) value. In cell cultures, the activity of SA-β-gal was defined as the ratio of SA-β-gal^+ cells, which was determined by counting the blue cells and dividing by the total number of observed cells. Further details are provided in the Supplemental Information.

RNA-Seq Analysis of H-NSCs and Proteomic Analysis of ESC-sEVs

RNA-seq analysis was performed by Shanghai Biotechnology (Shanghai, China). Purified libraries were quantified by a Qubit 2.0 fluorometer (Life Technologies, USA) and validated by an Agilent

Figure 7. ESC-sEVs Reverse Cognitive Aging and Rejuvenate H-NSC Senescence in C57BL/6 Mice

(A) Spatial learning and memory abilities were tested by an MWM test in 20 month-PBS and 20 month-sEV mice. n = 9 per group. ***$p < 0.001$. (B) Western blot analysis and quantification of Syp, Gap-43, PSD-95, and Syn-IIa in hippocampus of 20 month-PBS and 20 month-sEV mice. n = 6 per group. ***$p < 0.001$. (C) Western blot analysis of p-SMAD5, SMAD5, SMAD4, MYT1, Egln3, HIF-2α, NAMPT, and Sirt1 in isolated neurospheres of 20 month-PBS and 20 month-sEV mice. n = 3 per group. (D) SA-β-gal staining of hippocampus and quantification of hippocampal SA-β-gal activity in 20 month-PBS and 20 month-sEV mice. Scale bars, 250 μm. n = 6 per group. ***$p < 0.001$. (E) IF images for senescent H-NSCs ($p16^{INK4a+}$, red; $Sox2^+$, green) and the percentage of $Sox2^+/p16^{INK4a+}$ double-stained cells in whole $Sox2^+$ cells in the SGZ of 20 month-PBS and 20 month-sEV mice. Scale bars, 50 μm. n = 6 per group. ***$p < 0.001$. (F) SA-β-gal staining of isolated H-NSCs and the percentage of SA-β-gal^+ cells in 20 month-PBS and 20 month-sEV mice. Scale bars, 100 μm. n = 3 per group. ***$p < 0.001$. (G) Western blot analysis of $p16^{INK4a}$, γ-H2AX, p21, and p53 in isolated neurospheres of 20 month-PBS and 20 month-sEV mice. n = 3 per group. (H) IF images for hippocampal $Sox2^+$ (green) and $GFAP^+$ (red) cells and the number of $Sox2^+/GFAP^+$ double-stained cells in the SGZ of 20 month-PBS and 20 month-sEV mice. Scale bars, 50 μm. n = 6 per group. ***$p < 0.001$. (I) IF images for proliferating H-NSCs ($Sox2^+$, green; EdU^+, red) and the number of $Sox2^+/EdU^+$ double-stained cells in the SGZ of 20 month-PBS and 20 month-sEV mice. Scale bars, 50 μm. n = 6 per group. ***$p < 0.001$.

2100 bioanalyzer (Agilent Technologies, USA), and then sequenced on an Illumina HiSeq sequencer (Illumina, USA). The RNA-seq datasets have been deposited in the Gene Expression Omnibus (GEO) database under GEO: GSE158000. Proteomic analysis was performed by Shanghai Applied Protein Technology (Shanghai, China). LC-MS/MS analysis was performed on a Q Exactive mass spectrometer (Thermo Scientific). Further details are provided in the Supplemental Information.

RNA Pull-Down Assay

For MYT1 interference experiments, three pairs of shRNA sequences were designed and sequences are listed in Table S1. MYT1 silencing lentiviral particle (sh-MYT1) and sh-NCs were purchased from Hanbio Biotechnology (Shanghai, China). The shRNA was inserted into the lentivirus vector pHBLV-U6-MCS-CMV-ZsGreen-PGK-Puro (Hanbio Biotechnology) to silence MYT1. H-NSCs were transfected with sh-MYT1 or sh-NC under standard conditions using Polybrene, and 72 h later cells were subjected to selection with 1 μg/mL puromycin. Assays were performed after at least 10 days in selection.

Other Methods

Procedures related to the MWM test, IF staining, western blot analysis, qRT-PCR analysis, ESC-sEV uptake assay, and others are provided in the Supplemental Information.

Statistical Analysis

All data are presented as mean ± SD. An unpaired Student's t test was used to examine the inter-group differences, whereas one-way analysis of variance (ANOVA) was utilized to explore the heterogeneity among different groups, followed by a Bonferroni *post hoc* test in the absence of equivalent variance. A Kruskal-Wallis test and Mann-Whitney U test were applied for nonparametric analysis. A difference of $p < 0.05$ was deemed to be statistically significant.

SUPPLEMENTAL INFORMATION

Supplemental Information can be found online at https://doi.org/10.1016/j.ymthe.2020.09.037.

AUTHOR CONTRIBUTIONS

G.H. and Y.X. performed the experiments, ESC-sEV isolation, and proteomic analysis, and prepared the manuscript; B.C. and J.Z. performed animal experiments; L.G. and Y.C. performed data collection and analysis; and Q.L., Y.W., and Z.D. conceptualized the project, provided funding, supported the study material, and provided final approval of the manuscript.

CONFLICTS OF INTERESTS

The authors declare no competing interests.

ACKNOWLEDGMENTS

We sincerely thank Dr. Bin Hu, Xin Niu, Ji Yuan (Institute of Microsurgery on Extremities, Shanghai Jiao Tong University Affiliated Sixth People's Hospital), Dr. Qingwei Zhu, and Dr. Xiaozheng Ling (Department of Neurosurgery, Shanghai Jiao Tong University Affiliated Sixth People's Hospital) for technical assistance. This work was supported by the National Natural Science Foundation of China (project nos. 82071371, 81671209, and 81871833).

REFERENCES

1. Nguyen, H., Zarriello, S., Coats, A., Nelson, C., Kingsbury, C., Gorsky, A., Rajani, M., Neal, E.G., and Borlongan, C.V. (2019). Stem cell therapy for neurological disorders: a focus on aging. Neurobiol. Dis. *126*, 85–104.
2. Capilla-Gonzalez, V., Herranz-Pérez, V., and García-Verdugo, J.M. (2015). The aged brain: genesis and fate of residual progenitor cells in the subventricular zone. Front. Cell. Neurosci. *9*, 365.
3. Encinas, J.M., Michurina, T.V., Peunova, N., Park, J.H., Tordo, J., Peterson, D.A., Fishell, G., Koulakov, A., and Enikolopov, G. (2011). Division-coupled astrocytic differentiation and age-related depletion of neural stem cells in the adult hippocampus. Cell Stem Cell *8*, 566–579.
4. Bouab, M., Paliouras, G.N., Aumont, A., Forest-Bérard, K., and Fernandes, K.J. (2011). Aging of the subventricular zone neural stem cell niche: evidence for quiescence-associated changes between early and mid-adulthood. Neuroscience *173*, 135–149.
5. Childs, B.G., Durik, M., Baker, D.J., and van Deursen, J.M. (2015). Cellular senescence in aging and age-related disease: from mechanisms to therapy. Nat. Med. *21*, 1424–1435.
6. Ren, R., Ocampo, A., Liu, G.H., and Izpisua Belmonte, J.C. (2017). Regulation of stem cell aging by metabolism and epigenetics. Cell Metab. *26*, 460–474.
7. de Haan, G., and Lazare, S.S. (2018). Aging of hematopoietic stem cells. Blood *131*, 479–487.
8. Raabe, E.H., Lim, K.S., Kim, J.M., Meeker, A., Mao, X.G., Nikkhah, G., Maciaczyk, J., Kahlert, U., Jain, D., Bar, E., et al. (2011). BRAF activation induces transformation and then senescence in human neural stem cells: a pilocytic astrocytoma model. Clin. Cancer Res. *17*, 3590–3599.
9. Molofsky, A.V., He, S., Bydon, M., Morrison, S.J., and Pardal, R. (2005). Bmi-1 promotes neural stem cell self-renewal and neural development but not mouse growth and survival by repressing the $p16^{Ink4a}$ and $p19^{Arf}$ senescence pathways. Genes Dev. *19*, 1432–1437.
10. Molofsky, A.V., Slutsky, S.G., Joseph, N.M., He, S., Pardal, R., Krishnamurthy, J., Sharpless, N.E., and Morrison, S.J. (2006). Increasing $p16^{INK4a}$ expression decreases forebrain progenitors and neurogenesis during ageing. Nature *443*, 448–452.
11. Nishino, J., Kim, I., Chada, K., and Morrison, S.J. (2008). Hmga2 promotes neural stem cell self-renewal in young but not old mice by reducing $p16^{Ink4a}$ and $p19^{Arf}$ expression. Cell *135*, 227–239.
12. Neumann, B., Baror, R., Zhao, C., Segel, M., Dietmann, S., Rawji, K.S., Foerster, S., McClain, C.R., Chalut, K., van Wijngaarden, P., and Franklin, R.J.M. (2019). Metformin restores CNS remyelination capacity by rejuvenating aged stem cells. Cell Stem Cell *25*, 473–485.e8.
13. Théry, C., Witwer, K.W., Aikawa, E., Alcaraz, M.J., Anderson, J.D., Andriantsitohaina, R., Antoniou, A., Arab, T., Archer, F., Atkin-Smith, G.K., et al. (2018). Minimal information for studies of extracellular vesicles 2018 (MISEV2018): a position statement of the International Society for Extracellular Vesicles and update of the MISEV2014 guidelines. J. Extracell. Vesicles *7*, 1535750.
14. Adamiak, M., Cheng, G., Bobis-Wozowicz, S., Zhao, L., Kedracka-Krok, S., Samanta, A., Karnas, E., Xuan, Y.T., Skupien-Rabian, B., Chen, X., et al. (2018). Induced pluripotent stem cell (iPSC)-derived extracellular vesicles are safer and more effective for cardiac repair than iPSCs. Circ. Res. *122*, 296–309.
15. Basu, J., and Ludlow, J.W. (2016). Exosomes for repair, regeneration and rejuvenation. Expert Opin. Biol. Ther. *16*, 489–506.
16. Khan, M., Nickoloff, E., Abramova, T., Johnson, J., Verma, S.K., Krishnamurthy, P., Mackie, A.R., Vaughan, E., Garikipati, V.N., Benedict, C., et al. (2015). Embryonic

stem cell-derived exosomes promote endogenous repair mechanisms and enhance cardiac function following myocardial infarction. Circ. Res. *117*, 52–64.

17. Yabut, O., and Bernstein, H.S. (2011). The promise of human embryonic stem cells in aging-associated diseases. Aging (Albany NY) *3*, 494–508.
18. Bae, Y.U., Son, Y., Kim, C.H., Kim, K.S., Hyun, S.H., Woo, H.G., Jee, B.A., Choi, J.H., Sung, H.K., Choi, H.C., et al. (2019). Embryonic stem cell-derived mmu-miR-291a-3p inhibits cellular senescence in human dermal fibroblasts through the TGF-β receptor 2 pathway. J. Gerontol. A Biol. Sci. Med. Sci. *74*, 1359–1367.
19. Chen, B., Sun, Y., Zhang, J., Zhu, Q., Yang, Y., Niu, X., Deng, Z., Li, Q., and Wang, Y. (2019). Human embryonic stem cell-derived exosomes promote pressure ulcer healing in aged mice by rejuvenating senescent endothelial cells. Stem Cell Res. Ther. *10*, 142.
20. Smith, G.E. (2016). Healthy cognitive aging and dementia prevention. Am. Psychol. *71*, 268–275.
21. Liu, B., Liu, J., Zhang, J., Mao, W., and Li, S. (2019). Effects of autophagy on synaptic-plasticity-related protein expression in the hippocampus CA1 of a rat model of vascular dementia. Neurosci. Lett. *707*, 134312.
22. Sorrells, S.F., Paredes, M.F., Cebrian-Silla, A., Sandoval, K., Qi, D., Kelley, K.W., James, D., Mayer, S., Chang, J., Auguste, K.I., et al. (2018). Human hippocampal neurogenesis drops sharply in children to undetectable levels in adults. Nature *555*, 377–381.
23. Villeda, S.A., Luo, J., Mosher, K.I., Zou, B., Britschgi, M., Bieri, G., Stan, T.M., Fainberg, N., Ding, Z., Eggel, A., et al. (2011). The ageing systemic milieu negatively regulates neurogenesis and cognitive function. Nature *477*, 90–94.
24. Van Deun, J., Mestdagh, P., Agostinis, P., Akay, Ö., Anand, S., Anckaert, J., Martinez, Z.A., Baetens, T., Beghein, E., Bertier, L., et al.; EV-TRACK Consortium (2017). EV-TRACK: transparent reporting and centralizing knowledge in extracellular vesicle research. Nat. Methods *14*, 228–232.
25. Campisi, J. (1997). The biology of replicative senescence. Eur. J. Cancer *33*, 703–709.
26. Wang, X., Liu, C., Li, S., Xu, Y., Chen, P., Liu, Y., Ding, Q., Wahapu, W., Hong, B., and Yang, M. (2015). Effects of continuous passage on immunomodulatory properties of human adipose-derived stem cells. Cell Tissue Bank. *16*, 143–150.
27. Matsushita, F., Kameyama, T., Kadokawa, Y., and Marunouchi, T. (2014). Spatiotemporal expression pattern of Myt/NZF family zinc finger transcription factors during mouse nervous system development. Dev. Dyn. *243*, 588–600.
28. Vasconcelos, F.F., Sessa, A., Laranjeira, C., Raposo, A.A.S.F., Teixeira, V., Hagey, D.W., Tomaz, D.M., Muhr, J., Broccoli, V., and Castro, D.S. (2016). MyT1 counteracts the neural progenitor program to promote vertebrate neurogenesis. Cell Rep. *17*, 469–483.
29. Taniguchi, C.M., Finger, E.C., Krieg, A.J., Wu, C., Diep, A.N., LaGory, E.L., Wei, K., McGinnis, L.M., Yuan, J., Kuo, C.J., and Giaccia, A.J. (2013). Cross-talk between hypoxia and insulin signaling through Phd3 regulates hepatic glucose and lipid metabolism and ameliorates diabetes. Nat. Med. *19*, 1325–1330.
30. Yang, S., Ryu, J.H., Oh, H., Jeon, J., Kwak, J.S., Kim, J.H., Kim, H.A., Chun, C.H., and Chun, J.S. (2015). NAMPT (visfatin), a direct target of hypoxia-inducible factor-2α, is an essential catabolic regulator of osteoarthritis. Ann. Rheum. Dis. *74*, 595–602.
31. Ma, C., Pi, C., Yang, Y., Lin, L., Shi, Y., Li, Y., Li, Y., and He, X. (2017). Nampt expression decreases age-related senescence in rat bone marrow mesenchymal stem cells by targeting Sirt1. PLoS ONE *12*, e0170930.
32. Sanokawa-Akakura, R., Akakura, S., and Tabibzadeh, S. (2016). Replicative senescence in human fibroblasts is delayed by hydrogen sulfide in a NAMPT/SIRT1 dependent manner. PLoS ONE *11*, e0164710.
33. Colombo, M., Raposo, G., and Théry, C. (2014). Biogenesis, secretion, and intercellular interactions of exosomes and other extracellular vesicles. Annu. Rev. Cell Dev. Biol. *30*, 255–289.
34. Gong, L., Chen, B., Zhang, J., Sun, Y., Yuan, J., Niu, X., Hu, G., Chen, Y., Xie, Z., Deng, Z., et al. (2020). Human ESC-sEVs alleviate age-related bone loss by rejuvenating senescent bone marrow-derived mesenchymal stem cells. J. Extracell. Vesicles *9*, 1800971.
35. Sherry-Lynes, M.M., Sengupta, S., Kulkarni, S., and Cochran, B.H. (2017). Regulation of the JMJD3 (KDM6B) histone demethylase in glioblastoma stem cells by STAT3. PLoS ONE *12*, e0174775.
36. Ermolaeva, M., Neri, F., Ori, A., and Rudolph, K.L. (2018). Cellular and epigenetic drivers of stem cell ageing. Nat. Rev. Mol. Cell Biol. *19*, 594–610.
37. Maryanovich, M., Zahalka, A.H., Pierce, H., Pinho, S., Nakahara, F., Asada, N., Wei, Q., Wang, X., Ciero, P., Xu, J., et al. (2018). Adrenergic nerve degeneration in bone marrow drives aging of the hematopoietic stem cell niche. Nat. Med. *24*, 782–791.
38. Ocampo, A., Reddy, P., Martinez-Redondo, P., Platero-Luengo, A., Hatanaka, F., Hishida, T., Li, M., Lam, D., Kurita, M., Beyret, E., et al. (2016). *In vivo* amelioration of age-associated hallmarks by partial reprogramming. Cell *167*, 1719–1733.e12.
39. Neves, J., Sousa-Victor, P., and Jasper, H. (2017). Rejuvenating strategies for stem cell-based therapies in aging. Cell Stem Cell *20*, 161–175.
40. Chang, J., Wang, Y., Shao, L., Laberge, R.M., Demaria, M., Campisi, J., Janakiraman, K., Sharpless, N.E., Ding, S., Feng, W., et al. (2016). Clearance of senescent cells by ABT263 rejuvenates aged hematopoietic stem cells in mice. Nat. Med. *22*, 78–83.
41. Kodali, M., Castro, O.W., Kim, D.K., Thomas, A., Shuai, B., Attaluri, S., Upadhya, R., Gitai, D., Madhu, L.N., Prockop, D.J., and Shetty, A.K. (2019). Intranasally administered human MSC-derived extracellular vesicles pervasively incorporate into neurons and microglia in both intact and status epilepticus injured forebrain. Int. J. Mol. Sci. *21*, 181.
42. Aghajani Nargesi, A., Lerman, L.O., and Eirin, A. (2017). Mesenchymal stem cell-derived extracellular vesicles for kidney repair: current status and looming challenges. Stem Cell Res. Ther. *8*, 273.
43. Rohrbach, S., Simm, A., Pregla, R., Franke, C., and Katschinski, D.M. (2005). Age-dependent increase of prolyl-4-hydroxylase domain (PHD) 3 expression in human and mouse heart. Biogerontology *6*, 165–171.
44. Epstein, A.C., Gleadle, J.M., McNeill, L.A., Hewitson, K.S., O'Rourke, J., Mole, D.R., Mukherji, M., Metzen, E., Wilson, M.I., Dhanda, A., et al. (2001). *C. elegans* EGL-9 and mammalian homologs define a family of dioxygenases that regulate HIF by prolyl hydroxylation. Cell *107*, 43–54.
45. Stein, L.R., and Imai, S. (2014). Specific ablation of Nampt in adult neural stem cells recapitulates their functional defects during aging. EMBO J. *33*, 1321–1340.
46. Holloway, K.R., Calhoun, T.N., Saxena, M., Metoyer, C.F., Kandler, E.F., Rivera, C.A., and Pruitt, K. (2010). SIRT1 regulates Dishevelled proteins and promotes transient and constitutive Wnt signaling. Proc. Natl. Acad. Sci. USA *107*, 9216–9221.
47. Lie, D.C., Colamarino, S.A., Song, H.J., Désiré, L., Mira, H., Consiglio, A., Lein, E.S., Jessberger, S., Lansford, H., Dearie, A.R., and Gage, F.H. (2005). Wnt signalling regulates adult hippocampal neurogenesis. Nature *437*, 1370–1375.
48. Marchetti, B., and Pluchino, S. (2013). Wnt your brain be inflamed? Yes, it Wnt! Trends Mol. Med. *19*, 144–156.
49. Marchetti, B., Tirolo, C., L'Episcopo, F., Caniglia, S., Testa, N., Smith, J.A., Pluchino, S., and Serapide, M.F. (2020). Parkinson's disease, aging and adult neurogenesis: Wnt/β-catenin signalling as the key to unlock the mystery of endogenous brain repair. Aging Cell *19*, e13101.
50. Rong, Y., Liu, W., Lv, C., Wang, J., Luo, Y., Jiang, D., Li, L., Zhou, Z., Zhou, W., Li, Q., et al. (2019). Neural stem cell small extracellular vesicle-based delivery of 14-3-3t reduces apoptosis and neuroinflammation following traumatic spinal cord injury by enhancing autophagy by targeting Beclin-1. Aging (Albany NY) *11*, 7723–7745.
51. Théry, C., Zitvogel, L., and Amigorena, S. (2002). Exosomes: composition, biogenesis and function. Nat. Rev. Immunol. *2*, 569–579.
52. Hill, C.S. (2009). Nucleocytoplasmic shuttling of Smad proteins. Cell Res. *19*, 36–46.
53. Jovanovic, V.M., Salti, A., Tilleman, H., Zega, K., Jukic, M.M., Zou, H., Friedel, R.H., Prakash, N., Blaess, S., Edenhofer, F., and Brodski, C. (2018). BMP/SMAD pathway promotes neurogenesis of midbrain dopaminergic neurons *in vivo* and in human induced pluripotent and neural stem cells. J. Neurosci. *38*, 1662–1676.
54. Xin, H., Li, Y., and Chopp, M. (2014). Exosomes/miRNAs as mediating cell-based therapy of stroke. Front. Cell. Neurosci. *8*, 377.

55. Riquelme, P.A., Drapeau, E., and Doetsch, F. (2008). Brain micro-ecologies: neural stem cell niches in the adult mammalian brain. Philos. Trans. R. Soc. Lond. B Biol. Sci. *363*, 123–137.

56. Yousef, H., Czupalla, C.J., Lee, D., Chen, M.B., Burke, A.N., Zera, K.A., Zandstra, J., Berber, E., Lehallier, B., Mathur, V., et al. (2019). Aged blood impairs hippocampal neural precursor activity and activates microglia via brain endothelial cell VCAM1. Nat. Med. *25*, 988–1000.

57. Sun, F., Mao, X., Xie, L., Ding, M., Shao, B., and Jin, K. (2013). Notch1 signaling modulates neuronal progenitor activity in the subventricular zone in response to aging and focal ischemia. Aging Cell *12*, 978–987.

58. Kitayama, T., Yoneyama, M., Tamaki, K., and Yoneda, Y. (2004). Regulation of neuronal differentiation by *N*-methyl-D-aspartate receptors expressed in neural progenitor cells isolated from adult mouse hippocampus. J. Neurosci. Res. *76*, 599–612.

YMTHE, Volume *29*

Supplemental Information

ESC-sEVs Rejuvenate Aging Hippocampal NSCs by Transferring SMADs to Regulate the MYT1-Egln3-Sirt1 Axis

Guowen Hu, Yuguo Xia, Bi Chen, Juntao Zhang, Liangzhi Gong, Yu Chen, Qing Li, Yang Wang, and Zhifeng Deng

Supplemental Information

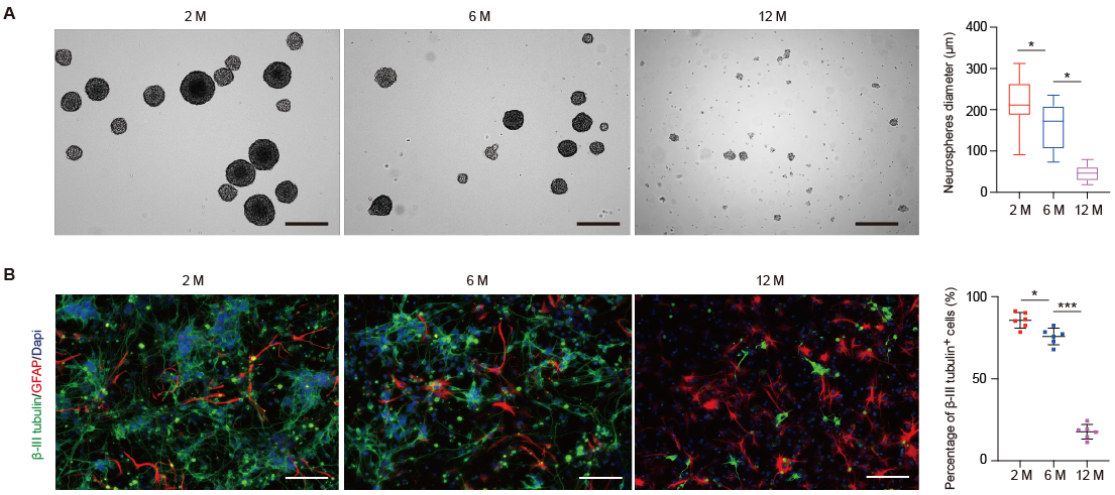

Figure S1. H-NSCs proliferation and neuronal-differentiation decreased with aging. (A) Neurospheres formation and quantification of neurospheres diameter in 2M, 6M, and 12M mice. Scale bar=300 μm; n=6 per group, *P<0.05. (B) IF images for β-III tubulin^{+} (green) and GFAP^{+} cells and the percentage of β-III tubulin^{+} cells in whole cells in 2M, 6M, 12M mice. Scale bar=100 μm, n=6 per group, *P<0.05, ***P<0.001.

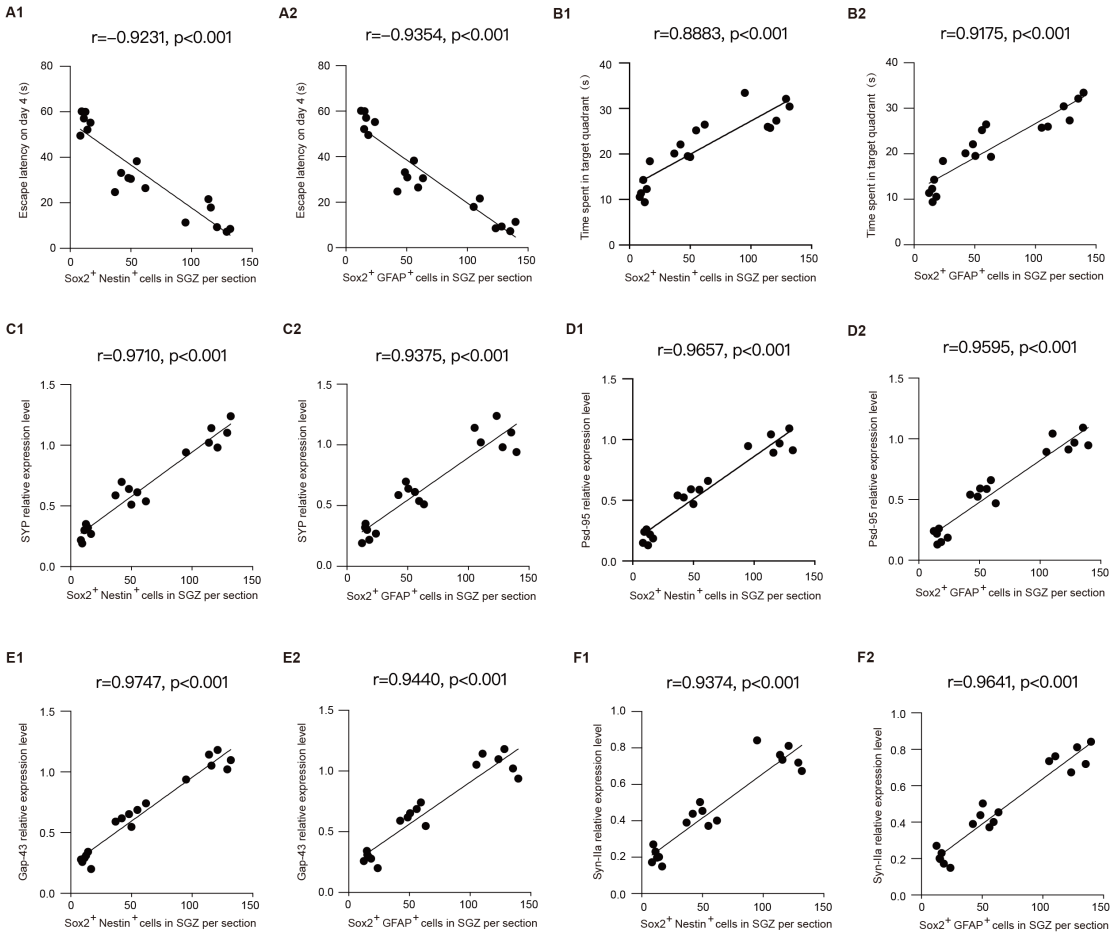

Figure S2. Correlation between the number of H-NSCs and cognitive function. (A) Correlation between the number of H-NSCs ($Sox2^+/Nestin^+$ cells and $Sox2^+/GFAP^+$ cells) in SGZ and the escape latency on day 4. n=6 per group. (B) Correlation between the number of H-NSCs in SGZ and the time spent in the target quadrant on day 5. n=6 per group. (C-F) Correlation between the number of H-NSCs in SGZ and the expression level of hippocampal synapse-related proteins (Syp, Psd-95, Gap-43, Syn-IIa). n=6 per group.

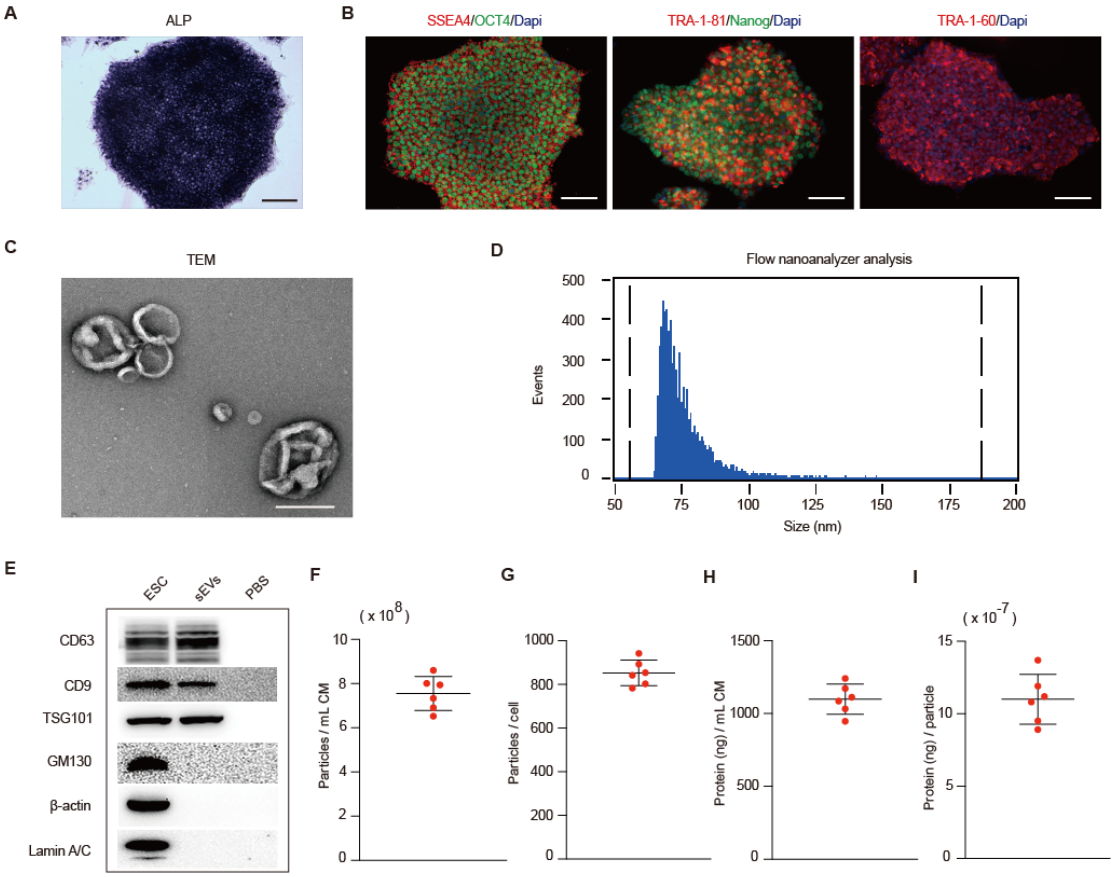

Figure S3. Characterization of ESCs and ESC-sEVs. (A) ALP staining of ESCs. Scale bar=150 μm. (B) IF images for OCT4, Nanog, TRA-1-81, TRA-1-60, and SSEA4 staining in ESCs. Scale bar=100 μm. (C) Morphology of ESC-sEVs observed by TEM. Scale bar=200 nm. (D) Particle size distribution of ESC-sEVs measured by nano-flow cytometer. (E) Western blot showed the presence of sEVs markers including CD63, CD9, and TSG101, and negative for GM130, β-actin, and Lamin A/C. (F)-(I) The yield of ESC-sEVs was evaluated in terms of particle concentration and protein concentration. The mean particle concentration of ESC-sEVs in condition medium (CM) was $7.06\times10^{8}\pm0.93\times10^{8}$ (particles/mL) (F) and 817.92±94.13 (particles/cell) (G), the mean protein concentration of ESC-sEVs in CM was 1127.49±81.47 (ng/mL) (H) and $11.43\times10^{-7}\pm1.57\times10^{-7}$ ng per particle (I). n=6 per group.

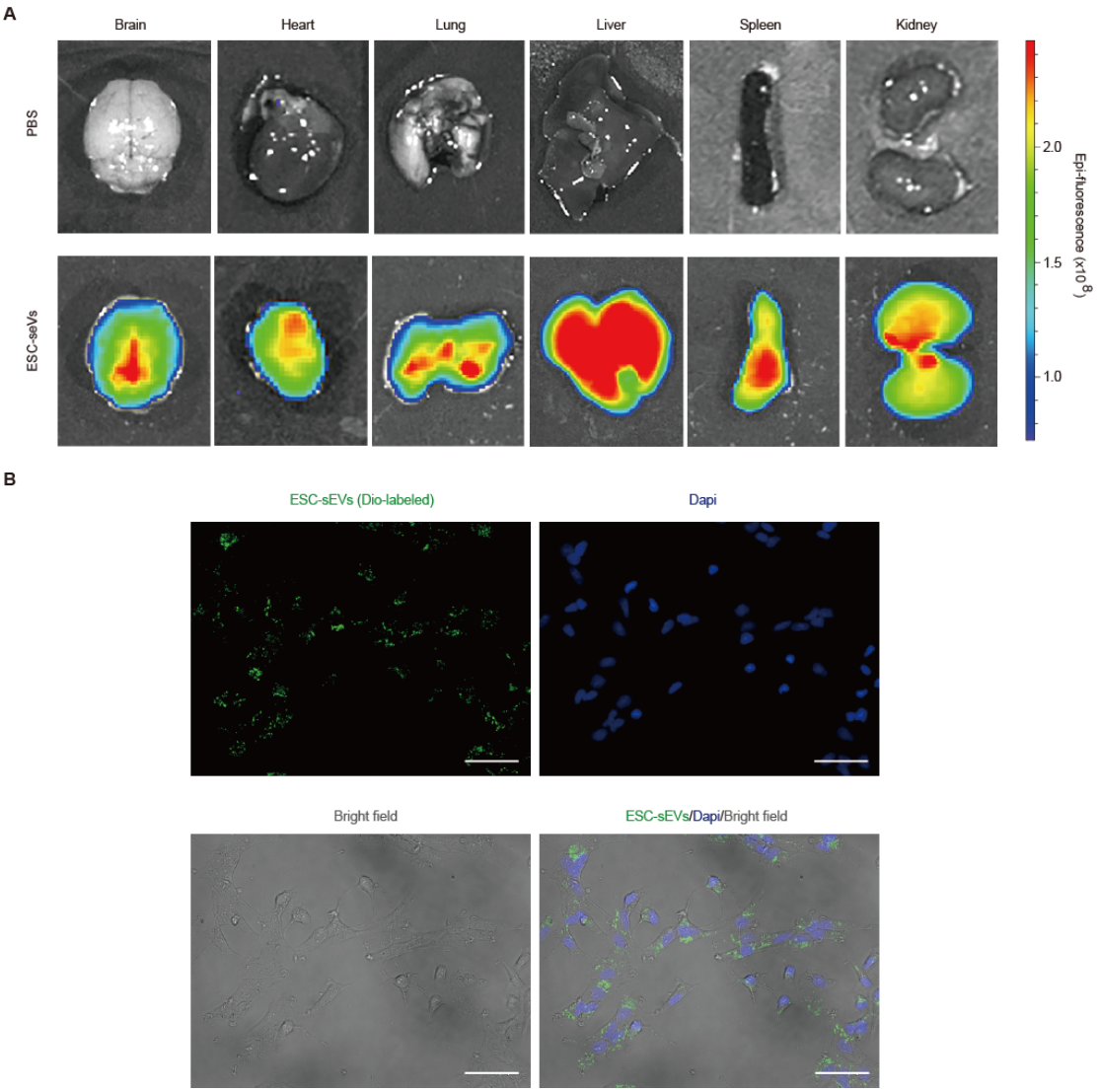

Figure S4. (A) *In vivo* fluorescence images of the distribution of DiR-labeled ESC-sEVs. DiR-labeled sEVs can distribute into brain, heart, lung, liver, spleen, and kidney at 24 hours after injection. n=3 per group. (B) IF for Dio-labeled ESC-sEVs (green) internalized by H-NSCs. Scale bar=50 μm, n=3 per group.

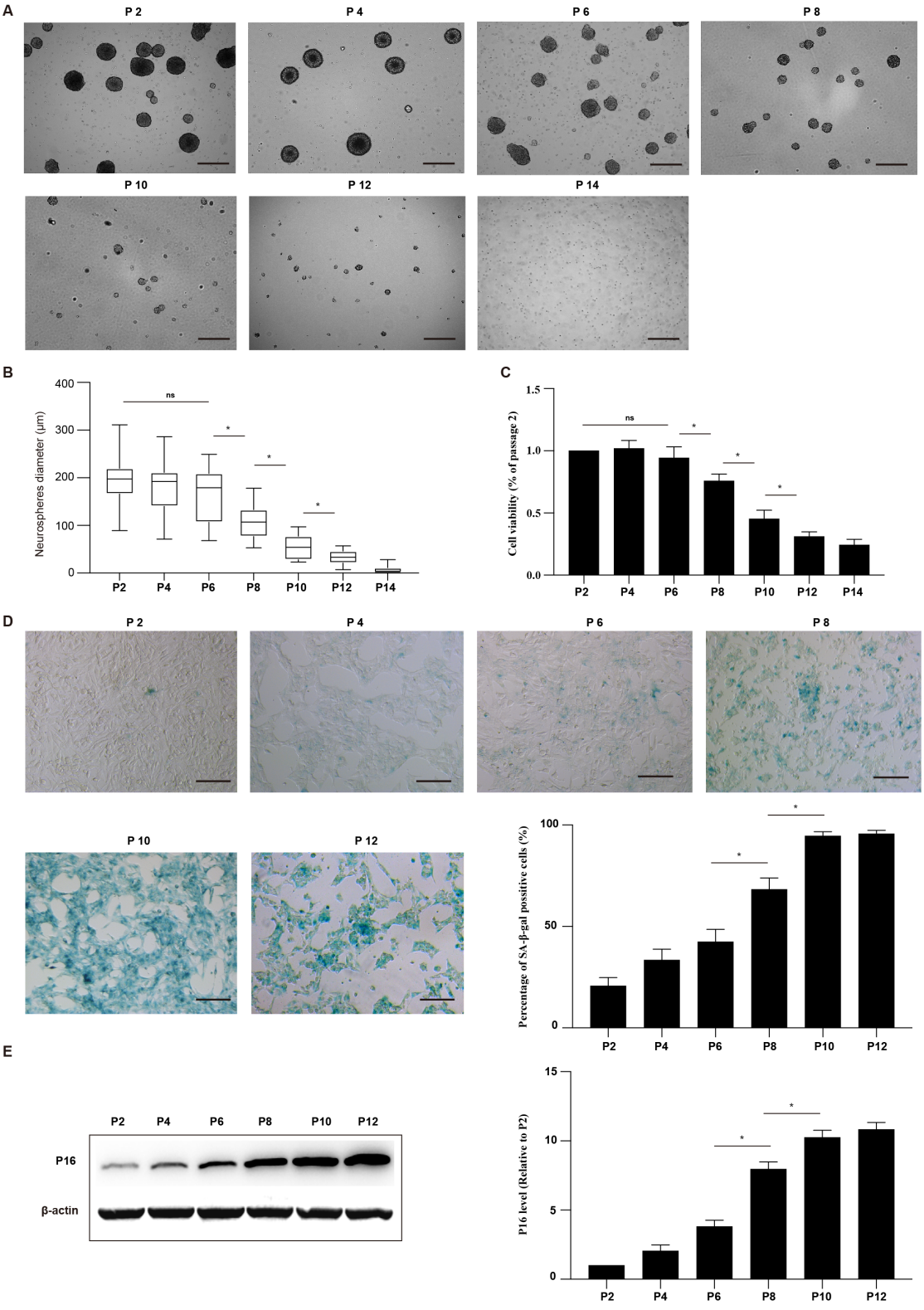

Figure S5. H-NSCs proliferation and senescence from passage 2 to 14 in vitro. (A) and (B) Neurospheres formation and quantification of neurospheres diameter in H-NSCs of

passage 2, 4, 6, 8, 10, 12, 14. Scale bar=300 μm; n=3 per group, *P<0.05. (C) Cell Counting Kit-8 (CCK-8) assay for H-NSCs of passage 2, 4, 6, 8, 10, 12, 14. n=3 per group, *P<0.05. (D) SA-β-gal staining and the percentage of SA-β-gal-positive cells in H-NSCs of passage 2, 4, 6, 8, 10, 12. Scale bar=100 μm, n=3 per group, *p<0.05. (E) Western blot analysis and quantification of $p16^{INK4a}$ in H-NSCs of passage 2, 4, 6, 8, 10, 12. n=3 per group, *p<0.05.

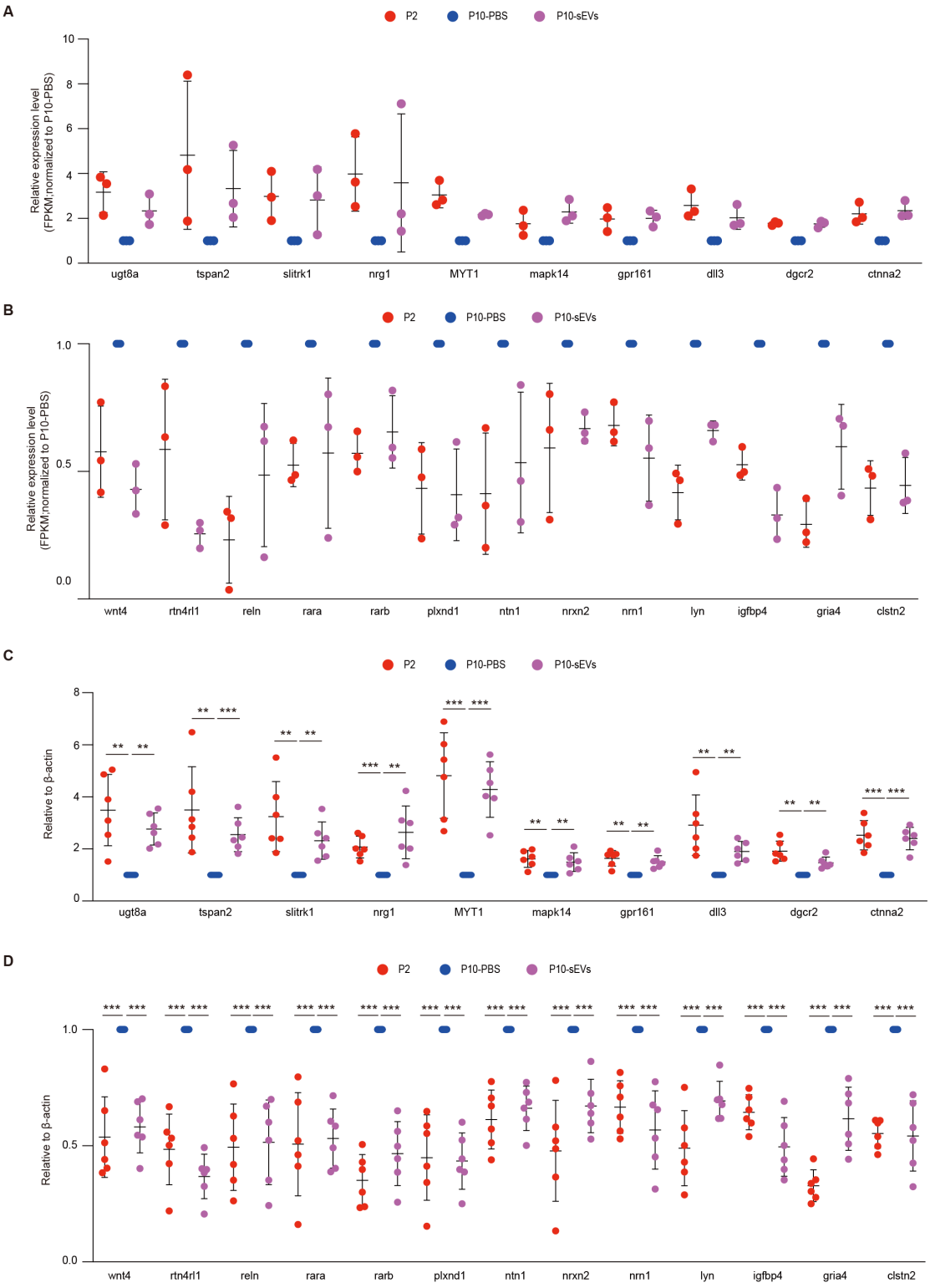

Figure S6. (A) and (B) Summary of the nervous system related 10 co-upregulated and 13 co-downregulated genes according to RNA-seq data from H-NSCs of P2 vs. P10-PBS and P10-sEVs vs. P10-PBS. (C) and (D) The relative expression of nervous system

related 10 co-upregulated and 13 co-downregulated genes were verified by RT-qPCR. n=6 per group, **P<0.01, ***P<0.001.

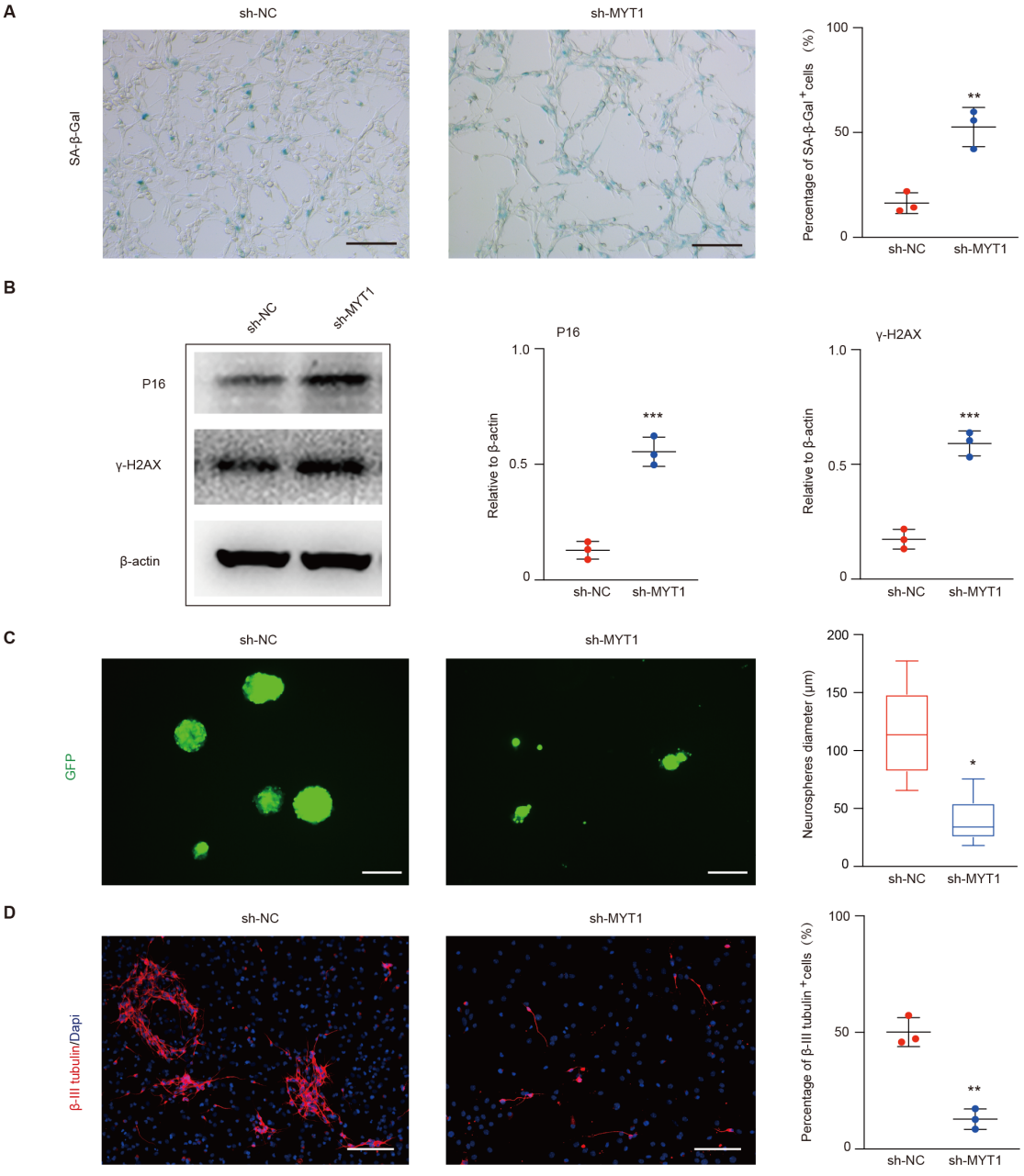

Figure S7. Knockdown of MYT1 induce H-NSCs senescence and impair proliferation and neuronal differentiation capacities. (A) Representative images of SA-β-gal staining and quantification of the percentage of SA-β-gal-positive cells in s hsh-NC NSCs and

sh-MYT1 NSCs. Scale bar=100 μm, n=3 per group, **P<0.01. (B) Western blot analysis and quantification of $p16^{INK4a}$ and γ-H2AX in sh-NC NSCs and sh-MYT1 NSCs. n=3 per group, ***P<0.001. (C) IF images for GFP labeled neurospheres and quantification of the diameter of neurospheres in sh-NC NSCs and sh-MYT1 NSCs. Scale bar=200 μm, n=3 per group, *P<0.05. (D) IF images for β-III $tubulin^+$ cells and the percentage of β-III $tubulin^+$ cells in whole cells in sh-NC NSCs and sh-MYT1 NSCs. Scale bar=100 μm, n=3 per group, **P<0.01.

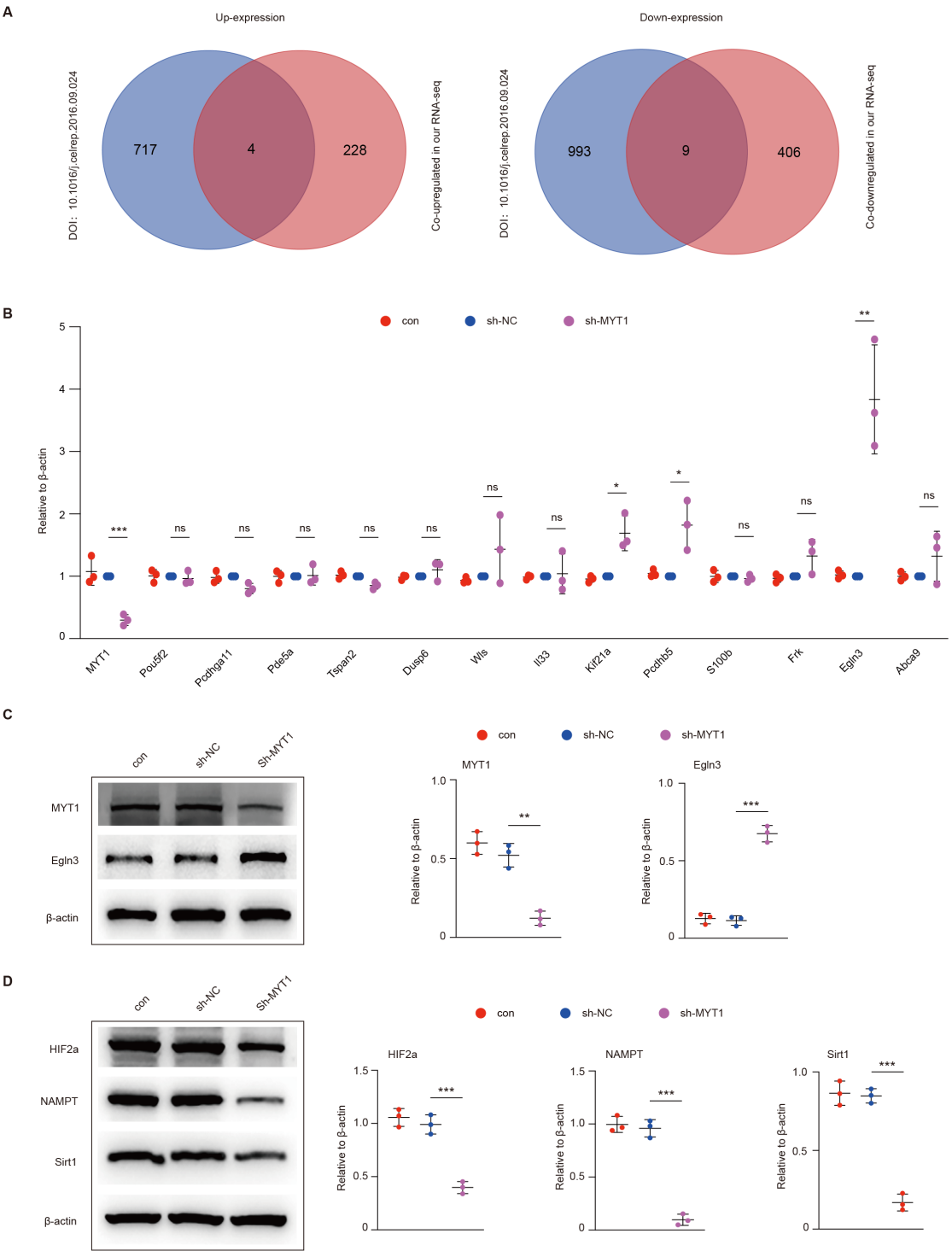

Figure S8. MYT1 inhibit Egln3 and upregulate HIF-2α, NAMPT, Sirt1 in H-NSCs. (A) Comparison of the co-upregulated and co-downregulated genes in H-NSCs of P2 vs. P10-PBS, P10-sEVs vs. P10-PBS with the published data (DOI : 10.1016/j.celrep.2016.09.024). (B) RT-qPCR verified the relative expression of Pou5f2,

Pcdhga11, Pde5a, Tspan2, Dusp6, Wls, Il33, Kif21a, Pcdhb5, S100b, Frk, Egln3, and Abca9 in sh-MYT1 NSCs and sh-NC NSCs. n=3 per group, *P<0.05, **P<0.01, ***P<0.001. (C) Western blot analysis and quantification of MYT1 and Egln3 in control NSCs, sh-NC NSCs, sh-MYT1 NSCs. n=3 per group, **P<0.01, ***P<0.001. (D) Western blot analysis and quantification of HIF-2α, NAMPT and Sirt1 in control NSCs, sh-NC NSCs, and sh-MYT1 NSCs. n=3 per group, ***P<0.001.

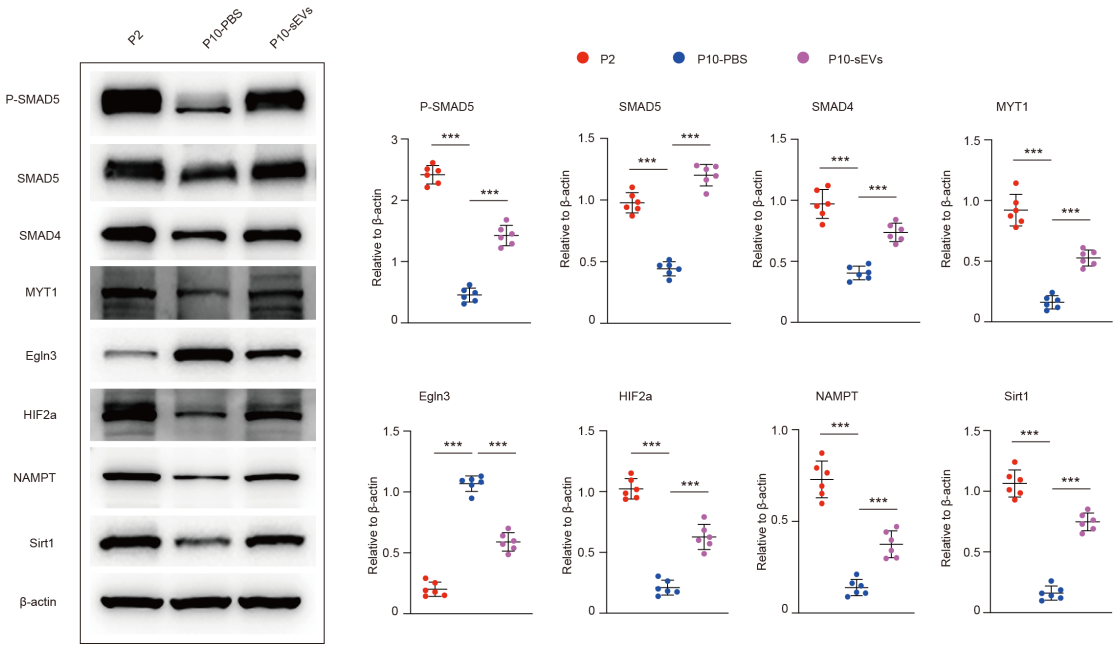

Figure S9. Western blot analysis and quantification of P-SMAD5, SMAD5, SMAD4, MYT1, Egln3, HIF-2α, NAMPT, and Sirt1 in H-NSCs of P2, P10-PBS, and P10-sEVs. n=6 per group, ***P<0.001.

Table S1. MYT1 gene interference sequence.

Interference fragment name	Sequence	
shRNA1	Top strand：	GATCCGCCCAGAGCTATCTAGTCCTAATTCAAGAGAT
		TAGGACTAGATAGCTCTGGGTTTTTTG
	Bottom	AATTCAAAAAACCCAGAGCTATCTAGTCCTAATCTCT
	strand：	TGAATTAGGACTAGATAGCTCTGGGCG
shRNA2	Top strand：	GATCCGAAGCAGCTTGAGGTTCCACCTTATTTCAAGA
		GAATAAGGTGGAACCTCAAGCTGCTTCTTTTTTG
	Bottom	AATTCAAAAAAGAAGCAGCTTGAGGTTCCACCTTATT
	strand：	CTCTTGAAATAAGGTGGAACCTCAAGCTGCTTCG
shRNA3	Top strand：	GATCCGAGGCAGAAAGAGGGAGCTCTCAATTTCAAG
		AGAATTGAGAGCTCCCTCTTTCTGCCTCTTTTTTG
	Bottom	AATTCAAAAAAGAGGCAGAAAGAGGGAGCTCTCAAT
	strand：	TCTCTTGAAATTGAGAGCTCCCTCTTTCTGCCTCG

Table S2. Sequences of primers used in RT-qPCR.

Gene name	Forward primer (5’ → 3’)	Reverse primer (5’ → 3’)
ugt8a	ACTCCATATTTCATGCTCCTGTG	AGGCCGATGCTAGTGTCTTGA
tspan2	TATCTGCTGCTCGGCTTCAAC	GTCCAAATGCAATAACGGCTG
slitrk1	GAAGGGGACTTACACGTAGACT	AGTGAGGGAATTGCCATGCAG
nrg1	ATGGAGATTTATCCCCCAGACA	GTTGAGGCACCCTCTGAGAC
MYT1	TGCAGACCTCAGTTGTCCTAC	TCCTCTTGGATACCAGGTGCT
mapk14	GGGACACCCCCTGCTTATCT	TCCCTGCTTTCAAAGGACTGG
gpr161	CTCACGCTTGGGGTCATTG	GAGCCAGATGTAGACGAGAGC
dll3	CTGGTGTCTTCGAGCTACAAAT	TGCTCCGTATAGACCGGGAC
dgcr2	ATGCTGCACAGACCTGTCAG	TCCTGGGCTAGGACGAAGC
ctnna2	TTCAGAGCACTTCCACTACCT	CTGCTTCCACTCCCGATTGG
wnt4	AGACGTGCGAGAAACTCAAAG	GGAACTGGTATTGGCACTCCT
rtn4rl1	CTGCCAGGCACACAACTTTG	TGTTGGAGTAGATCCAGAGGG
reln	TTACTCGCACCTTGCTGAAAT	CAGTTGCTGGTAGGAGTCAAAG
rara	ATGTACGAGAGTGTGGAAGTCG	ACAGGCCCGGTTCTGGTTA
rarb	GCAGTGCGTGGACACATGA	GGCAGGGAGAGTCCTCTGAT
plxnd1	TCGCTGCCAATCCCTAATAAGA	TGACCTGGTTTGGAACTGTTG
ntn1	CAGCCTGATCCTTGCTCGG	GCGGGTTATTGAGGTCGGTG
nrxn2	TTAAACAGCGAAGTAGGGTC	GCCAGTGTGATCTCGTCA
nrn1	GCGGTGCAAATAGCTTACCTG	CGGTCTTGATGTTCGTCTTGTC

lyn	GTGACATTGTGGTGGCCTTAT	ACCATTCCCCATGCTCTTCTA
igfbp4	AGAAGCCCCTGCGTACATTG	TGTCCCCACGATCTTCATCTT
gria4	GTTTTCTGGATTTTGGGGACTCG	AAGAGACCACCTATTTGAACGC
clstn2	CCTCCTGCGGAAGGACTTTG	TGGGCCAGTCATTAGTCACCA
Pou5f2	GGTCTTCAAACGTCTTCCCTC	CCCATACTTGGTCGCACCAT
Pcdhga11	CTGATCCCGCTGTGCATTTTC	TGCCTACGAAGAAGCCTTTATCT
Pde5a	CGGCCTACCTGGCATTCTG	GCAAGGTCAAGTAACACCTGATT
Dusp6	ATAGATACGCTCAGACCCGTG	ATCAGCAGAAGCCGTTCGTT
Wls	ATGGCTGGGGCAATTATAGAAAA	GGGTGCTGGAGCGATCAAG
Il33	TCCAACTCCAAGATTTCCCCG	CATGCAGTAGACATGGCAGAA
Kif21a	AAGATCGAAGGTTGCCATATCTG	CAGCTCCGGTTTGTCCATAGG
Pcdhb5	CAGGCAAGTGATTCCTTTCCT	ATTGCTGTTTGTCATGGTCAGA
S100b	TGGTTGCCCTCATTGATGTCT	CCCATCCCCATCTTCGTCC
Frk	ACCCGAAGCCATTCGTACTAA	AGCACCTGTCATACCACTGTA
Egln3	AGGCAATGGTGGCTTGCTATC	GCGTCCCAATTCTTATTCAGGT
Abca9	TCGATAGATGCAGTGAGAGTCA	CACAAGGAGCTGAATGGTCTTT
β-actin	GGCTGTATTCCCCTCCATCG	CCAGTTGGTAACAATGCCATGT

Table S3. Models and methods in article.

	Models	Methods
In vivo	SAMP8 mice: (1) 2M, 6M, 12M; (2)6M, 12M-PBS, 12M-sEVs	(1) Morris water maze; (2) Western blot for Syp, Psd-95, Gap-43, Syn-IIa; (3) IF staining for Sox2, Nestin, GFAP, DCX, PCNA, $p16^{INK4a}$; (4) SA-β-gal staining
	C57/BL mice: 20M-PBS, 20M-sEVs	(1) Morris water maze; (2) Western blot for Syp, Psd-95, Gap-43, Syn-IIa; (3) IF staining for Sox2, GFAP, DCX, Edu, $p16^{INK4a}$; (4) SA-β-gal staining
Ex vivo	SAMP8 mice: H-NSCs isolated from 6M, 12M-PBS, 12M-sEVs	(1) SA-β-gal staining; (2) Western blot for $p16^{INK4a}$, γ -H2AX, P21, and P53; (3) proliferation assay: IF staining for Edu; (4) neuronal-differentiation assay: IF staining for β-Tubulin III and GFAP

		(5) Western blot for P-SMAD5, SMAD5, SMAD4, and MYT1, Egln3, HIF-2α, NAMPT, Sirt1
	C57/BL mice: H-NSCs isolated from 20M-PBS, 20M-sEVs	(1) SA-β-gal staining; (2) Western blot for $p16^{INK4a}$, γ -H2AX, P21, and P53; (3) Western blot for P-SMAD5, SMAD5, SMAD4, and MYT1, Egln3, HIF-2α, NAMPT, Sirt1
In vitro	H-NSCs isolated from 2-weeks C57/BL mice, replicative senescence model （passage 2 -10）	(1) SA-β-gal staining; (2) Western blot for $p16^{INK4a}$, γ -H2AX, P21, and P53; (3) proliferation assay: IF staining for Edu; neurospheres formation assay; (4) neuronal-differentiation assay: IF staining for β-Tubulin III and GFAP; (5) RNA-seq analysis; (6) RT-qPCR; (7) Lentiviral knockdown; (8) chromatography-tandem mass spectrometry (LC-MS/MS) analysis; (9) Western blot for P-SMAD5, SMAD5, SMAD4, and MYT1, Egln3, HIF-2α, NAMPT, Sirt1

Supplemental Materials & Methods

ESC culture

The human embryonic stem cells (ESC; H9) were provided by the Institute of Biochemistry and Cell Biology of Chinese Academy of Sciences (Shanghai, China). The ESC were cultured in ncEpic hPSC medium (NO. RP01001; Nuwacell Biotechnologies, China) on a Nuwacell™-Vitronectin (NO. RP01002-A; Nuwacell) coated plate under the standard conditions of 5%CO2 and 37°C in humidified incubator. The medium was changed daily and cells were passaged at 80~90% confluence. ESCs identification was performed by ALP staining and immunofluorescence staining (IF) for markers (Nanog, OCT4, SSEA4, TRA-1-60, and TRA-1-81) in the ESC colonies.

ESC-sEVs isolation and identification

ESC-sEVs isolation

Embryonic stem cells derived small extracellular vesicles (ESC-sEVs) were isolated by differential ultracentrifugation protocols from ESCs condition medium (ESC-CM) according to the MISEV2018 guideline. Briefly, ESC-CM was centrifuged at 300×g for 10 min to remove dead cells and 2000×g for 20 min to remove cellular debris and apoptotic bodies. Then, the supernatant was centrifuged at 10,000×g for 30 min and filtered through 0.22 μm sterilized filter (Millipore, Bedford, MA, USA) to remove large EVs. Next, the supernatant was subjected to ultracentrifugation at 100,000×g for 114 min by using a SW 32 Ti Rotor Swinging Bucket rotor (K factor of 256.8, 28536 rpm; Beckman Coulter, Fullerton, CA) to pellet ESC-sEVs. After removing the

supernatant, the ESC-sEVs pellet was washed with PBS and followed by a second ultracentrifugation at 100,000×g for 114 min. All centrifugation steps were performed at 4°C. Finally, the pellet was re-suspended in PBS and stored at -80°C.

Transmission Electron Microscope (TEM)

The morphology of ESC-sEVs was observed by TEM (JEM 1400, Tokyo, Japan). Briefly, a total of 10μL ESC-sEVs enriched solution was placed on a formvar-carbon coated grid (300 meshes) and left to dry at room temperature for 20min. Then, ESC-sEVs was washed with PBS and fixed in 1% glutaraldehyde for 5 min. Next, ESC-sEVs was washed with water and stained with saturated aqueous uranyl oxalate for 5 min. Finally, the grid was dried at room temperature for 10 min and then imaged.

Size distribution and particle concentration

The size distribution and particle concentration of ESC-sEVs were measured by using the nano-flow cytometer (N30 Nanoflow Analyzer, NanoFCM Inc., Xiamen, China) as described previously[1]. Briefly, the side scatter intensity (SSI) was measured by the loading of the standard polystyrene nanoparticles (200 nm) with a concentration of 1.58 $\times 10^8$/mL to the nano-flow cytometer. Next, isolated ESC-sEVs sample diluted with 1000-fold PBS (for a nanoparticle concentration of approximately 5×10^9/mL) was loaded to the nano-flow to measure the SSI. Finally, the concentration of EVs was calculated according to the ratio of SSI to particle concentration in the standard polystyrene nanoparticles. For size measurement, standard silica nanoparticles with mixed size (68nm, 91nm, 113nm, 155nm) were load to the nano-flow cytometer to

generate a standard cure, followed by the loading of sEVs sample. The size distribution was calculated according to the standard cure.

Protein concentration

The protein concentration of ESC-sEVs was quantified by Pierce BCA Protein Assay Kit (Thermo Scientific) according to the product manual. Briefly, 200 μL of the WR solution was loaded into each well of a 96-well plate. Next, 10 μL of the ESC-sEVs sample was added. Finally, the plate was incubated at 37°C for 30 min and the absorbance was detected at 562 nm. A standard curve was used to determine the protein concentration of each ESC-sEVs sample.

sEVs markers

The expression of sEVs markers such as CD9, CD63, and TSG-101 was analyzed by western blot. GM130, β-actin, and Lamin A/C were also detected to determine the purity of ESC-sEVs. Briefly, the ESC-sEVs pellet was routine ultracentrifugation as described above. ESC-sEVs protein was harvested by using RIPA lysis buffer supplemented with protease inhibitor cocktail (Roche). Then, the protein concentration of ESC-sEVs was detected by using the Pierce BCA Protein Assay Kit as described above. Next, protein was separated by sodium dodecyl sulfatepolyacrylamide gel electrophoresis and transferred to polyvinylidene fluoride membranes (Millipore). The membranes were blocked with 5% non-fat milk for 1 h and incubated overnight at 4 °C with the following antibodies: rabbit monoclonal anti-β-actin (1:1,000; Abcam, NO. ab179467), rabbit monoclonal anti-CD9 (1:1,000; Abcam, NO. ab92726), rabbit monoclonal anti-CD63 (1:1,000; Abcam, NO. ab134045), mouse monoclonal anti-

TSG-101 (1:1,000; Abcam, NO.ab83), mouse polyclonal anti-GM130 (1:500; Abcam, NO.ab169276), Rabbit polyclonal anti-Lamin A/C (1:1000; Servicebio, NO. GB11407). Membranes were then incubated with HRP-conjugated secondary antibodies (1:3,000; Cell Signaling Technology) at room temperature for 1 h. The immunoreactive bands were visualized using ECL (Thermo Fisher Scientific) and imaged with a FluorChem M Fluorescent Imaging System (ProteinSimple, Santa Clara, CA, USA).

In vivo ESC-sEVs migration into brain

To determine the migration of ESC-sEVs into the brain, ESC-sEVs were labeled with the Molecular Probes' Vybrant (Life Technologies, NY, Cat No. D12731) 1,1'-dioctadecyl-3,3,3',3'-tetramethylindotricarbocyanine iodide (DiR) according to the protocol as previously described with small modification[2]. Briefly, ESC-sEVs were incubated with DiR fluorescent dye under room temperature for 15 minutes, then were loaded at the bottom of an iodixanol cushion (0%, 20%, 30%, and 50%) and centrifuged at 100,000×g for 114 min (SW 32-Ti Rotor) to separate them from the free unbound dye. The DiR-labeled ESC-sEVs were collected from the interphase between 20% and 30% and washed in PBS and centrifuged at 100,000×g for 114 min (SW 32-Ti Rotor). SAMP8 mice (n = 3) were intravenously administered with fresh purified DiR-labeled ESC-sEVs (1×10^{10} particles/ml,100μl), followed by euthanasia and ex vivo imaging of dissected organs at 24 hours after application. Bio-distribution of DiR-labeled ESC-sEVs was examined by using IVIS Spectrum (Perkin Elmer). The harvested organs were imaged for 1-2 seconds (excitation 710 nm, emission 760 nm). The data were analyzed with the IVIS software (Living Image Software for IVIS).

Morris Water Maze

Morris water maze (MWM) test was employed to assess spatial learning and memory abilities of rats as described previously[3]. The latency to escape onto the platform was recorded as the performance of spatial learning. Mice were trained once a day over four consecutive days. In each trial, mice were gently released into the water with their head facing opposite of the platform, and were given a maximum of 60s to find the submerged platform. For mice that could not find the platform within 60s, they were guided to stay on it for 15s, and the score of 60s was given to such mice. To assess spatial memory, a spatial probe trial was performed on day 5 of the training trial. The platform was removed and mice were placed in water opposite to the target quadrant, and allowed to swim freely for 60s. The percentage of time that mice spent in the target quadrant within 60s was recorded. The Shanghai Xinran Mdt InfoTech Ltd (Shanghai, China) SuperMaze animal behavior record and analysis system was used for data collection and analysis.

Immunofluorescence (IF) staining

Mice were anesthetized and perfused transcardially with saline, then followed by 4% paraformaldehyde (PFA; 4.3 g/L NaOH, 40 g/L paraformaldehyde, 18.8 g/L NaH2PO4.H20). The brains were removed and post-fixed overnight in 4% PFA, and then dehydrated in 20% and 30 % sucrose at 4 °C, respectively. Each brain was embedded in OCT and cut every sixth 20-μm-thick coronal sections on a freezing microtome (Leica CM 1950; Leica Biosystem, Heidelberg, Germany). Cells were fixed by 4% PFA for 15 min. Brain sections or cultured cells were incubated with 0.3% Triton

X-100 for 30 min and 5 % bovine serum albumin (BSA; Sigma, St. Louis, MO, USA) for 1 h, and then incubated overnight at 4 °C with the following antibodies: rabbit polyclonal anti-Sox2 (1:100; Cell Signaling Technology, NO. cst2748), mouse monoclonal anti-GFAP (1:100; Abcam, NO. ab10062), rabbit monoclonal anti-β-Tubulin III (1:100; Abcam, NO.ab18207), mouse monoclonal anti-Nestin (1:100; Abcam, NO. ab6142), rabbit polyclonal anti-DCX (1:100; Abcam, ab18723), mouse monoclonal anti-$p16^{INK4a}$ (1:200; Invitrogen, NO.MA5-17142), mouse monoclonal anti-PCNA (1:100; Abcam, NO. ab29), rabbit polyclonal anti-Nanog (1:100; Abcam, NO.ab109250), rabbit polyclonal anti-OCT4 (1:100; Abcam, NO.ab19857), mouse monoclonal anti-SSEA4 (1:100; Abcam, NO.ab16287), mouse monoclonal anti-TRA-1-60 (1:100; Abcam, NO.ab16288), mouse monoclonal anti-TRA-1-81 (1:100; Abcam, NO.ab16289). Followed by three times of rinse in 0.1 M PBS (pH 7.4) before the incubation with secondary antibodies (1:400; Invitrogen) including Alexa Fluor® 594 goat anti-rabbit or anti-mouse IgG (H+L) or Alexa Fluor® 488 goat anti-rabbit or anti-mouse IgG (H + L) for 1 h at room temperature, protected from light. EdU^+ cells were stained by using Click-iT Edu Alexa Fluor 488 or 594 Imaging Kit (Life Technologies) following the manufacturer's protocol. Nuclei was visualized by using 2 μM DAPI (Sigma). Images were acquired using the Leica DM6B microscope (Leica Microsystems, Milan, Italy). The number of positively stained cells were performed using the Image J software (National Institutes of Health, Bethesda, MD, USA).

H-NSCs isolation and cultivation

H-NSCs were isolated from mice hippocampus as described previously. Briefly, hippocampus was separated from brain and minced by scissors, then treated with enzyme cocktail solution (papain (2.5 U/mL), DNase (250 U/mL) and dispase (1U/mL)) at 37°C for 1 h. Later mixed with an equal volume of percoll solution and centrifuged at 20,000 g for 30 min at 18°C. H-NSCs located in the lower layer fraction were harvested and washed three times with DMEM/F12, and resuspended in complete H-NSCs medium: DMEM/F12 medium supplemented with 2% B27 (Gibco Life Technologies), 1% penicillin/streptomycin (Gibco Life Technologies), 20 ng/ml epidermal growth factor (EGF, ProSpec), 20 ng/ml basic fibroblast growth factor (bFGF, ProSpec), and 5 μg / ml heparin (Sigma-Aldrich). Cells were seeded in a culture plate and the medium was fifty percent replaced every 2 days.

In vitro ESC-sEVs uptake assay

ESC-sEVs were labeled with fluorescent carbocyanine dye (Dio, Life Technologies) for 30 min at 37 °C as our previously described. The labeled ESC-sEVs were loaded at the bottom of an iodixanol cushion (0%, 20%, 30%, and 50%) and centrifuged at 100,000×g for 114 min (SW 32-Ti Rotor) to separate them from the free unbound dye. The DiR-labeled ESC-sEVs were collected from the interphase between 20% and 30% and washed in PBS and centrifuged at 100,000×g for 114 min (SW 32-Ti Rotor). H-NSCs were incubated with Dio-labeled ESC-sEVs (1×10^{10} particles/mL) for 12 h. After that, culture medium was discarded and the cells were rinsed twice with PBS. H-

NSCs were fixed, nucleus was stained with DAPI. Images were acquired using the Leica DM6B microscope.

Senescence-associated β-galactosidase (SA-β-gal) staining

SA-β-gal staining of brain sections and NSCs were performed using the SA-β-gal staining kit (Beyotime Biotechnology, Cat No.C0602). According to manufacturer's protocol, brain sections or cell cultures were fixed and then stained with SA-β-gal staining solution for 16-18 h at 37 °C (without CO_2), ice-cold PBS was used to stop the enzymatic reaction. Images of brain sections were acquired using the Leica DM6B microscope, the activity of SA-β-gal for hippocampus was evaluated by means of a ROD (relative optical density) value. ROD of SA-β-gal positive cells was obtained after transformating mean gray values (obtained by Image Pro Plus software) into ROD via the formula: ROD = log (256/mean gray). In cell cultures, neurospheres were dissociated with Accutase (Sigma-Aldrich), 20,000 cells were plated into individual wells of poly-L-lysine (Sigma-Aldrich) coated 24-well plates and incubated in complete NSCs medium for 6 hours, then H-NSCs were fixed and stained for SA-β-gal activity, at least ten images of NSCs were acquired under the phase-contrast microscope (Leica Microsystems). The activity of SA-β-gal was defined as the ratio of SA-β-gal positive cells, which determined by counting the blue cells and dividing by the total number of observed cells.

Effects of ESC-sEVs on H-NSCs senescence, proliferation, and differentiation

We applied replicative senescence model to detect effects of ESC-sEVs on H-NSCs senescence. Briefly, H-NSCs were incubated with 1×10^{10} particles/mL ESC-sEVs or

an equal volume of PBS from passage 2 to passage 10. NSCs senescence was detected by SA-β-gal staining and western blot. For Edu incorporation assay, neurospheres were dissociated and 20,000 cells were plated into individual wells of ultralow-binding 24-well plates and incubated in complete NSCs medium for 4 days, and then administered EdU (10uM) for 4 hours. Neurospheres were plated on poly-L-lysine (Sigma-Aldrich) coated 24-well plates and adhered for 6 hours. Then, Neurospheres were fixed and immunofluorescence staining to calculate the percentage of EdU^+ cells in whole cells, at least ten images of neurospheres were acquired. For CCK8 assay, 20,000 cells were plated into individual wells of ultralow-binding 24-well plates and incubated in complete NSCs medium for 4 days, CCK-8 solution (per 10 μL in 100 μL medium) was added into medium and incubated for 2 h at 37°C. The amount of formazan dye generated by cellular dehydrogenase activity was measured for absorbance at 450 nm by using a microplate reader. The optical density values of each well represented the survival/proliferation of H-NSCs. For neurospheres formation assay, 20,000 cells were plated into individual wells of ultralow-binding 24-well plates and incubated in complete NSCs medium for 6 days, the diameter of neurospheres were counted under a phase-contrast microscope or fluorescent microscope, at least ten images of neurospheres were acquired. For the differentiation assay, neurospheres were dissociated and 50,000 cells were plated on poly-L-lysine coated 48-well plates. Cells were cultured with the differentiation medium: neural basal (NB) medium (Gibco Life Technologies) supplemented with 2% B27 and 1% fetal bovine serum (Gibco Life Technologies), and cultured for 5 days, the medium was half-changed every other day.

Cells were fixed and immunofluorescence staining for β-Tubulin III and GFAP to calculate the percentage of β-Tubulin III $^{+}$ cells in whole cells. Images were acquired using the Leica DM6B microscope, and at least ten images were acquired.

RNA-sequencing analysis

RNA-seq analysis was performed by Shanghai Biotechnology Corporation (Shanghai, China). In brief, total RNA was isolated using RNeasy mini kit (Qiagen, Germany). Paired-end libraries were synthesized by using the TruSeq™ RNA Sample Preparation Kit (Illumina, USA) following TruSeq™ RNA Sample Preparation Guide. The poly-A containing mRNA molecules were purified using Poly-T oligo-attached magnetic beads. Following purification, the mRNA is fragmented into small pieces using divalent cations under 94°C for 8 min. The cleaved RNA fragments are copied into first strand cDNA using reverse transcriptase and random primers. This is followed by second strand cDNA synthesis using DNA polymerase I and RNase H. These cDNA fragments then go through an end repair process, the addition of a single 'A' base, and then ligation of the adapters. The products are then purified and enriched with PCR to create the final cDNA library. Purified libraries were quantified by Qubit® 2.0 Fluorometer (Life Technologies) and validated by Agilent 4200 bioanalyzer (Agilent Technologies, USA) to confirm the insert size and calculate the mole concentration. Cluster was generated by cBot with the library diluted to 10 pM and then were sequenced by using the Next Generation Sequencing (NGS) on the Illumina HiSeq 2500. Raw Reads were checked Seqtk to select the clean Reads. Genome mapping was carried out by using Hisat2 (version: 2.0.4). Using Stringtie (version:1.3.0) to calculate genes's fragments,

and perl was used to calculate Fragments Per Kilobase of exon model per Million mapped reads (FPKM) of every gene.

Proteomic analysis of ESC-sEVs

The proteomic analysis was performed by the Shanghai Applied Protein Technology Company (Shanghai, China) as our previous described. In brief, sEVs samples were suspended in SDT lysis buffer. The proteins were separated on 12.5% SDS-PAGE gel and protein bands were visualized by Coomassie Blue R-250 staining. 200 μg of proteins for each sample were incorporated into 30 μl SDT buffers. The detergent, DTT and other low-molecular-weight components were removed using UA buffer by repeated ultrafiltration. Then 100 μl iodoacetamide was added to block reduced cysteine residues and the samples were incubated for 30 min in darkness. The filters were washed with 100 μl UA buffer three times and then 100 μl 25mM NH4HCO3 buffer twice. Finally, the protein suspensions were digested with 4 μg trypsin (Promega) overnight at 37 °C, and the resulting peptides were collected as a filtrate. The peptides of each sample were desalted on C18 Cartridges, concentrated by vacuum centrifugation and reconstituted in 40 μl of 0.1% (v/v) formic acid. Liquid chromatography-tandem mass spectrometry (LC-MS/MS) analysis was performed on a Q Exactive mass spectrometer (Thermo Scientific) that was coupled to Easy nLC (Thermo Fisher Scientific) for 240 min. The mass spectrometer was operated in positive ion mode. The MS data were analyzed using MaxQuant software version 1.5.3.17.

Real-time quantification polymerase chain reaction (RT-qPCR) analysis

Targeted gene expression analyses were performed by RT-qPCR analysis as described before[4]. Briefly, total RNA was isolated using QIAzol Lysis Reagent and RNeasy Mini Columns (QIAGEN, Valencia, CA). DNase treatment was applied to degrade contaminating genomic DNA using an on-column RNase-free DNase solution (QIAGEN, Valencia, CA). RNA quantity and purity were confirmed with a Nanodrop spectrophotometer (Thermo Scientific, Wilmington, DE). Reverse transcriptase was performed using the High-Capacity cDNA Reverse Transcription Kit (Applied Biosystems by Life Technologies, Foster City, CA). PCR reactions were run using the ABI Prism 7900HT Real Time System (Applied Biosystems, Carlsbad, CA) with SYBR green (QIAGEN, Valencia, CA). The data was analyzed using the cycle threshold (Ct) value. Each experiment was performed in triplicate. The primer sequences used in this study are listed in Table S2.

Western blot

H-NSCs whole protein was harvested by using RIPA lysis buffer supplemented with protease inhibitor cocktail (Roche) and Phosphatase inhibitor cocktail (Roche). The protocols for protein concentration mesurement and western blot were described above. The following antibodies were usde: $p16^{INK4a}$ (1:1,000), rabbit monoclonal anti-P21 (1:1,000; Abcam, NO.ab109199), rabbit polyclonal anti-P53 (1:1,000; Abcam, NO.ab131442), rabbit monoclonal anti-Phospho-Histone H2A.X (Ser139) (γ-H2AX; 1:200; Cell Signaling Technology, NO. cst9718), mouse monoclonal anti-SYP (1:1,000; Abcam, NO.ab8049), mouse monoclonal anti-Psd-95 (1:1,000; Abcam, NO.ab13552),

mouse monoclonal anti-Gap-43 (1:500; Santa Cruz, NO.sc-17790), mouse monoclonal anti-Syn-IIa (1:500; Santa Cruz, NO.sc-136086), rabbit monoclonal anti-SMAD5 (phospho S463 + S465) (P-SAMD5; 1:2000; Abcam, NO.ab92698), rabbit monoclonal anti-SMAD5 (1:2000; Abcam, NO.ab40771), rabbit monoclonal anti-SMAD4 (1:5000; Abcam, NO.ab40759), rabbit monoclonal anti-NAMPT (1:1000; Abcam, NO.ab236874), rabbit monoclonal anti-Egln3 (1:2000; Abcam, NO.ab184714), rabbit polyclonal anti-MYT1 (1:1,000; Abcam, NO.ab82844), rabbit polyclonal anti-HIF2α (1:1,000; Abcam, NO.ab199), rabbit monoclonal anti-Sirt1 (1:1000; Abcam, NO.ab189494), rabbit monoclonal anti-β-actin (1:1,000; Abcam, NO.ab179467). The bands were imaged with a FluorChem M Fluorescent Imaging System and the gray value was analyzed by Image J software.

References

1. Tian, Y, Ma, L, Gong, M, Su, G, Zhu, S, Zhang, W*, et al.* (2018). Protein Profiling and Sizing of Extracellular Vesicles from Colorectal Cancer Patients via Flow Cytometry. *ACS nano* **12**: 671-680.
2. Zhu, Q, Ling, X, Yang, Y, Zhang, J, Li, Q, Niu, X*, et al.* (2019). Embryonic Stem Cells-Derived Exosomes Endowed with Targeting Properties as Chemotherapeutics Delivery Vehicles for Glioblastoma Therapy. *Adv Sci (Weinh)* **6**: 1801899.
3. Costa-Mattioli, M, Gobert, D, Harding, H, Herdy, B, Azzi, M, Bruno, M*, et al.* (2005). Translational control of hippocampal synaptic plasticity and memory by the eIF2alpha kinase GCN2. *Nature* **436**: 1166-1173.
4. Hu, GW, Li, Q, Niu, X, Hu, B, Liu, J, Zhou, SM*, et al.* (2015). Exosomes secreted by human-induced pluripotent stem cell-derived mesenchymal stem

cells attenuate limb ischemia by promoting angiogenesis in mice. *Stem Cell Res Ther* **6**: 10.